Journal of
Polymer & Composites
https://journals.stmjournals.com/jopc

ISSN: 2321-2810 (Online)
ISSN: 2321-8525 (Print)
Volume 14, Issue 2, 2026
DOI (Journal): 10.37591/JoPC

Review JoPC

An Integrated Simulation Framework for Predicting Dielectric Breakdown and Electrical Aging in Epoxy-Silica Composite Insulation Systems

Digvijay B Kanase[1,*], Arun Thorat[2], Swapnil Patil[3], Suraj Pawar[4], Sachin P Jadhav[5], Vishal Patil[6]

Abstract

This paper provides a combined computation approach in forecasting the dielectric breakdown and electrical aging within epoxy-silica composite of insulation system. The approach will consist of a three-complementary methodology (a combination of computing electric field using the finite element analysis, estimation of the probability of failures or breakdowns using Weibull statistics, and prediction of degradation tendencies using artificial neural networks). The epoxy-silica composites are of 10-40 volumes fillers. The simulations include both electrical and thermal stresses which have field strengths of 8-25 kV/mm together with temperatures of 300-340 K keeping in mind the aging mechanisms of up to 30,000 hours. Findings indicate local field enhancement of 24.7% at filler-matrix interfaces indicating the need of field examination in designing insulation properly. The voltage endurance coefficient is 7.2 showing great sensitivity to electrical stress. Maximum filler amount of 28.6% will provide an 32.5% longer life of insulation than unfilled epoxy. The root mean square error of the artificial neural network in predicting breakdown strength is 0.047 kV/mm which is a 42% reduction over the traditional linear regression. The means and B10 of design conditions of the reliability analysis are 40.9 years and 27.7 years, respectively which can be useful in insulation optimization, conditions estimation and remaining life estimation in high voltage equipment.

Keywords: Epoxy-silica composites, dielectric breakdown, electrical aging, finite element analysis, artificial neural networks, insulation reliability, weibull statistics

***Author for Correspondence**
Digvijay B Kanase
E-mail id: digvijaykanase91@yahoo.in

[1]Assistant Professor, Department of Electrical Engineering, Dr. D. Y. Patil Institute of Technology, Pune, Maharashtra, India
[2]Associate Professor, Department of Electrical Engineering, Kasegaon Education Society's Rajarambapu Institute of Technology, Affiliated to Shivaji University, Sakharale, Maharashtra, India
[3]Assistant Professor, Department of Electrical Engineering, Walchand College of Engineering, Sangli, Maharashtra, India
[4]Assistant Professor, Department of Electrical Engineering, Annasaheb Dange College of Engineering and Technology, Maharashtra, India
[5,6]Assistant Professor, Department of Electrical Engineering, Kasegaon Education Society's Rajarambapu Institute of Technology, Affiliated to Shivaji University, Sakharale, Maharashtra, India

Received Date: March 05, 2026
Accepted Date: March 21, 2026
Published Date: April 07, 2026

Citation: Digvijay B Kanase, Arun Thorat, Swapnil Patil, Suraj Pawar, Sachin P Jadhav, Vishal Patil. An Integrated Simulation Framework for Predicting Dielectric Breakdown and Electrical Aging in Epoxy-Silica Composite Insulation Systems. Journal of Polymer & Composites. 2026; 14 (2): 339–376p.

INTRODUCTION

High-voltage insulations transfer Polymer composite materials have proved to be invaluable because of their high dielectric characteristics, thermal stability and flexibility in mechanical installations. Inorganic reinforced epoxy resins, especially with silica, have captured specific attention in terms of using it in power transformers, rotating machines, cable terminations, and switchgear. The rising level of compactness, efficiency and reliability of electrical power system, requires high-quality insulation materials that can easily handle the rising electrical stress and offer extended service. [1-3]

Polymer composite electrical aging is a complicated process due to the interactions of electrical, thermal and environmental stresses. These are partial discharge, space charge, chemical degradation and interfacial degradation of the polymer matrix and of filler particles. These aging phenomena are highly nonlinear and multi-factorial and they have many material-dependent characteristics which make their understanding and prediction extremely challenging. [4-6]

Recent methods of insulation aging test use accelerated life tests which expose materials to increased stress in order to speed up the degradation tests [7-9]. Although useful in some ways, such procedures are subject to limitations such as uncertainties in extrapolation, time consuming processes, cost and the possibility of introducing degradation mechanisms which are not graphical of the actual service conditions. Computational simulation is also a complementary method, which allows the study of aging processes in detail without much experimental programs. [10-12]

This study creates a conjoint MATLAB-based simulation framework which is a synergistic combination of data-driven and physical modelling. The strategy adds significant gaps that they have in the literature by combining finite element analysis to compute fields, statistical analysis to determine failure, and artificial intelligence to predict aging trends. The framework has its specifications on epoxy-silica composite systems with the consideration of realistic material properties, geometry arrangements and work conditions. [13-15]

The main goals are: (1) formulate precise models of electric field distribution in non-homogeneous composite, (2) provide sound statistical procedures to break-down probabilities estimation, (3) apply Artificial neural networks to predict the ageing behaviour through the use of artificial neural networks and (4) check the integrated framework with the existing physical models. The importance is found in the minimization of the use of large-scale experimental tests and offering more insight into the aging processes and contributing to the design of insulation optimization to increase its reliability and effectiveness.

LITERATURE REVIEW AND GAPS

Fields of systematic study of the effects of ageing of field strength and duration on polymer composites have serve as further advances in investigating electrical aging in polymer composites. The comprehensive study by Wang and colleagues (2026) of epoxy/silicon carbide composites that were exposed to conditions of different electrical aging conditions showed important observations on the mechanisms of degrading the properties of these materials. Their results reveal that the values of permittivity and loss tangent have a high dependence on increased aging electric field and the aging time that is accompanied by high levels of trap density in the composite structure. Notably, the breakdown strength of old ones was significantly lower than new ones, whereas the nonlinear coefficient of old age was actually getting better with the age- a fact that is explained through altered charge transport mechanism. The observations allow developing a fundamental basis on understanding the long-term stability of field grading materials, and have a direct influence on the parameterization of aging models in computational frameworks.[16-20]

Innovations in epoxy insulation, including the voltage endurance properties of insulation through non-sinusoidal waves have re-emerged especially in the new utilizations of high-frequency power electronics use. Most recent studies on square wave voltage conditions have shown the validity of inverse power law response when considering lifetime quality with voltage endurance coefficients depending strongly on frequency, amplitude, and temperature. This study fills a very important gap in the literature since most of the earlier works considered are situation based on power frequency or DC conditions and thus the power frequency converter fed insulation is not characterized very well. [21-25]

Another key topic in the study of composite insulation is the optimization of the silica filler content so that the recent research can give subtle insights into the relationships between concentrations and various properties in the studies. Systematically, Kokayeva et al. (2023) examined epoxy composites

ISSN: 2321-2810 (Online), ISSN: 2321-8525 (Print)

with micro silica as a filler material in dosage levels of 2 to 15 wt% and found the best loading levels at different mechanical and physical properties. Their findings reveal that 2 wt% micro silica level attained the highest improvements that includes 45% improvement in adhesion and toughness, 21% enhancement in tensile strength, 5% improvement in elastic modulus and 32 % improvement in coating impact strength. Such results indicate the criticality of optimization of filler loading, too much filler loading may result in agglomeration, and degradation of property.

Similar studies by Mogila et al. (2023) used sol-gel synthesis to produce amine-curing polymer silica composites with SiO 2 content in 0.5 to 10 wt%. When mass fractal silica nanoparticles formed during synthesis, the reinforcing effects to the epoxy polymer matrix results were observed with 5 wt% SiO 2 being the best amount to give maximum effective activation energy in degradation of the particle. This concentration dependent phenomenon demonstrates how performance of a given composite is affected by expandable filler loading largely supporting the necessity of systematic optimization in the design of insulations.[26-30]

The development of simple particle dispersion to engineered filler architectures is a major phenomenon in the technology of composite insulations. The study was the first attempt to investigate silica-titania (SiO 2 @ TiO 2) core-shell nanoparticles in amine-cured epoxy composites and revealed how thermal treatment of particles affected dielectric properties (Chaudhary, Vryonis, and Andritsch, 2024). Their thorough description on the basis of transmission electron microscopy, Fourier transform infrared spectroscopy, Raman spectroscopy, differential scanning calorimetry and broadband dielectric spectroscopy exposed that the temperature at which they are calcined is a primary determining factor in shell density and molecular order. It is worth noting that the incorporation of untreated fillers led to a reduction in bulk real permittivity when the fillers were calcined, and vice versa. The fact that, in the imaginary permittivity spectral analysis, there is observation of extra ω relaxation in the Nano composites indicating that there was no longer the same molecular dynamics of the epoxy matrix when nanoparticles had been added- this was observed with immense implications in interpreting the interfacial processes in composite dielectrics.

Surface modification approaches are constantly developing, and silane coupling agents are still the most common methods of increasing the compatibility between fillers and matrices. The comprehensive review with different approaches to the introduction of silicon dioxide into epoxy matrices prepared (but withdrawn) by Wang et al. (2022) reported a variety of silicon dioxide incorporation methods, namely sol-gel and direct mixing with the surface-modified nanoparticles. The critical nature of hydroxyl group management on the surfaces of the particles was highlighted because remaining hydroxyls may give the particle it unwanted acidity and influence the reactivity of resin.

The design of real-world insulation systems should stand up to electrical stress and be capable of withstanding the environment, decades of use. A remarkable study by Haider et al. (2025) was carried out to determine the performance of silica fiber/epoxy wave-transparent composite under one and two years of real and accelerated aging, respectively, of the material with the Hallberg-Peck model. This publication gives the previously unmatched quantitative information on the evolution of the property: dielectric constant improved by 4.34% and 30.63% (already 3.2) after one year and after 20 years, correspondingly); dielectric loss additionally rose by 5.6% and 22.83 % (up to 0.035); highest moisture absorption awakened 3.1% after 20 years; tensile strength was also lowered to 136.48 MPa, compressive strength was lowered to Most importantly, the state of the properties deteriorated substantially, whereas the composite showed a sufficiently high level of functionality, as the micro scale characterization of the latter showed gradually weaker interfacial bonding. The data is essential in tests which would verify long-term aging predictions about computation frameworks.

Phenomena that cause pre-breakdown are important as they are required to predict the dielectric breakdown accurately. In CiNii Research (2026), the electrical tree propagation and suppressions under epoxy/Nano-silica composites were studied through synchrotron radiation using micro-X-ray computed tomography. The morphological variations were remarkable when evaluated by the three-dimensional structural analysis: electrical tree branches were observed to be developed in neat epoxy resin, whereas bush-type trees were typical of the Nano composite. Quantitative analysis based on fractal distance dimension estimates of reconstructed CT scans and dielectric breakdown modelling proved that the model nano-silica insertion is at the root of a qualitative change in tree propagation. Moreover, the decay of dielectric breakdown voltage when humidity treatment was performed was markedly absorbed over with the Nano composite which points to the preservative motion of well-dispersed nanoparticles against environmental degradation.[31-34]

Author(s)	Year	Application	Methodology	Key Results	Long relevance to present study
de Santos and Sanz-Bobi	2023	Condition monitoring of high-voltage insulators under polluted environmental conditions	Ensemble Machine Learning Techniques	Achieved classification accuracy exceeding 90% for contamination severity levels under adverse operating conditions	Establishes a reliable data-driven framework for insulation health assessment, demonstrating the capability of machine learning models to accurately classify contamination levels, which is essential for predictive maintenance of high-voltage insulation systems
Kumar et al.	2025	Optimization of pineapple fiber/SiO_2 reinforced epoxy nanocomposites	Artificial Neural Network (ANN)-based optimization	Identified optimal processing conditions leading to significant enhancement in dielectric strength and overall material performance	Demonstrates the effectiveness of ANN in optimizing composite insulation materials, directly supporting the application of intelligent models for improving dielectric properties in epoxy-silica-based insulation systems
Haiba and Gad	2024	Fault identification in high-voltage ceramic insulators	Artificial Neural Networks (ANN)	Achieved high classification accuracy (94.2%) in detecting defective insulators	Validates the robustness and precision of ANN models in identifying insulation defects, reinforcing their applicability in fault diagnostics and reliability assessment of high-voltage insulation infrastructure
Qiu and Ge	2025	Non-destructive evaluation of aging and failure in insulating coatings	Ultrasonic Guided Waves integrated with Machine Learning (hybrid physics-informed and data-driven approach)	Enabled early-stage degradation detection with high predictive accuracy across various insulation coatings	Highlights the significance of integrating physical sensing techniques with machine learning for early detection of insulation aging, which is critical for enhancing the lifespan and reliability of insulation systems
Emdadi et al.	2025	Monitoring and diagnostics of high-voltage cable insulation systems in smart grid environments	Comprehensive Review of Machine Learning Applications	Identified transition from time-based to condition-based maintenance using ML techniques	Provides a comprehensive contextual foundation for the adoption of machine learning in insulation monitoring, supporting the development of intelligent, adaptive maintenance strategies for modern power systems

ISSN: 2321-2810 (Online), ISSN: 2321-8525 (Print)

Important Literature

Gaps:

The literature review mostly focuses only on electrical or environmental aging and little has been done to investigate the synergistic impact of electro-thermal-mechanical stress on epoxy-silica composite materials over a longer period of time (more than 30,000 hours).

- There is not yet any validated computational framework that incorporates finite element analysis of field calculation, Weibull statistics based failure probability estimation, and machine learning based prediction of degradation trends into a single process of conducting comprehensive assessment of insulation life.
- Contradictory optimal concentration is reported in filler optimization studies of 2 wt% to 35 wt% based upon the preference of focus on mechanical or thermal or electrical properties without a multi-objective approach to optimization having been reported.
- Most current studies lack systematic validation against multiple independent literature sources and classical models (IEC 60243-1) which removes the generalizability as well as practical application of research results.

METHODOLOGY

The simulated structure adheres to a modular structure represented in Figure 1. The input parameters such as material properties, operating conditions and geometrical configurations are used to drive three concurrent computational modules, which are: (1) electric field computation using finite elements, (2) statistical Weibull modelling to estimate the probability of breakdown, and (3) artificial neural networks to predict the trends in aging. A feedback loop allows optimization of models in accordance with validation measures. The combined results give overall performance evaluation, such as breakdown feasibility, estimations of life and field distribution and quantitative performance results. The system of insulation uses a parallel-plate capacitor type as illustrated in Figure 2 using epoxy-silica composite as the dielectric material. The physical layout is that of a 5 mm thick insulation layer between electrodes of the high voltage and ground. The annexed circuit represents the equivalent circuit; polymer capacitance (C_ρ) and polymer resistance (R_ρ) will be 150 pF and 10 G, respectively and contact resistance, R_c, will be half-an ohm. This arrangement allows the use of DC voltages to 50 kV at electric field stresses of between 8-25 kV/mm.

Theoretical Frame Work

Electric Field Analysis in Heterogeneous Composites

The distribution of electric fields in polymer composites with filler particles necessitates the consideration of the heterogeneity on the different scales. The stock to flow equation is the Poisson equation.

$$\nabla.(\epsilon\nabla\phi) = -\rho \tag{1}$$

with, ϕ , ε, and ρ, being the electric potential, permittivity grown, and space charge density, respectively. In case of one-dimensional where there is no space charge, this even reduces to:

$$\frac{d}{dx}\left(\varepsilon\frac{dV}{dx}\right) = 0 \tag{2}$$

The Maxwell equation of effective permittivity of polymer composite is obtained as:

$$\frac{\varepsilon_{eff}-\varepsilon_m}{\varepsilon_{eff}+2\varepsilon_m} = v_f\frac{\varepsilon_{eff}-\varepsilon_m}{\varepsilon_{eff}+2\varepsilon_m} \tag{3}$$

With ε_{eff}, ε_f, ε_m, and v_f being the effective permittivity, filler permittivity, matrix permittivity, and filler volume fraction respectively.

Electrical Aging Models

Combined stress approaches are the use of aging to process it. The model of electro-thermal aging is followed:

$$L = L_0\left(\frac{E}{E_0}\right)^{-n} exp\left[\frac{E_a}{k}\left(\frac{1}{T}-\frac{1}{T_0}\right)\right] \tag{4}$$

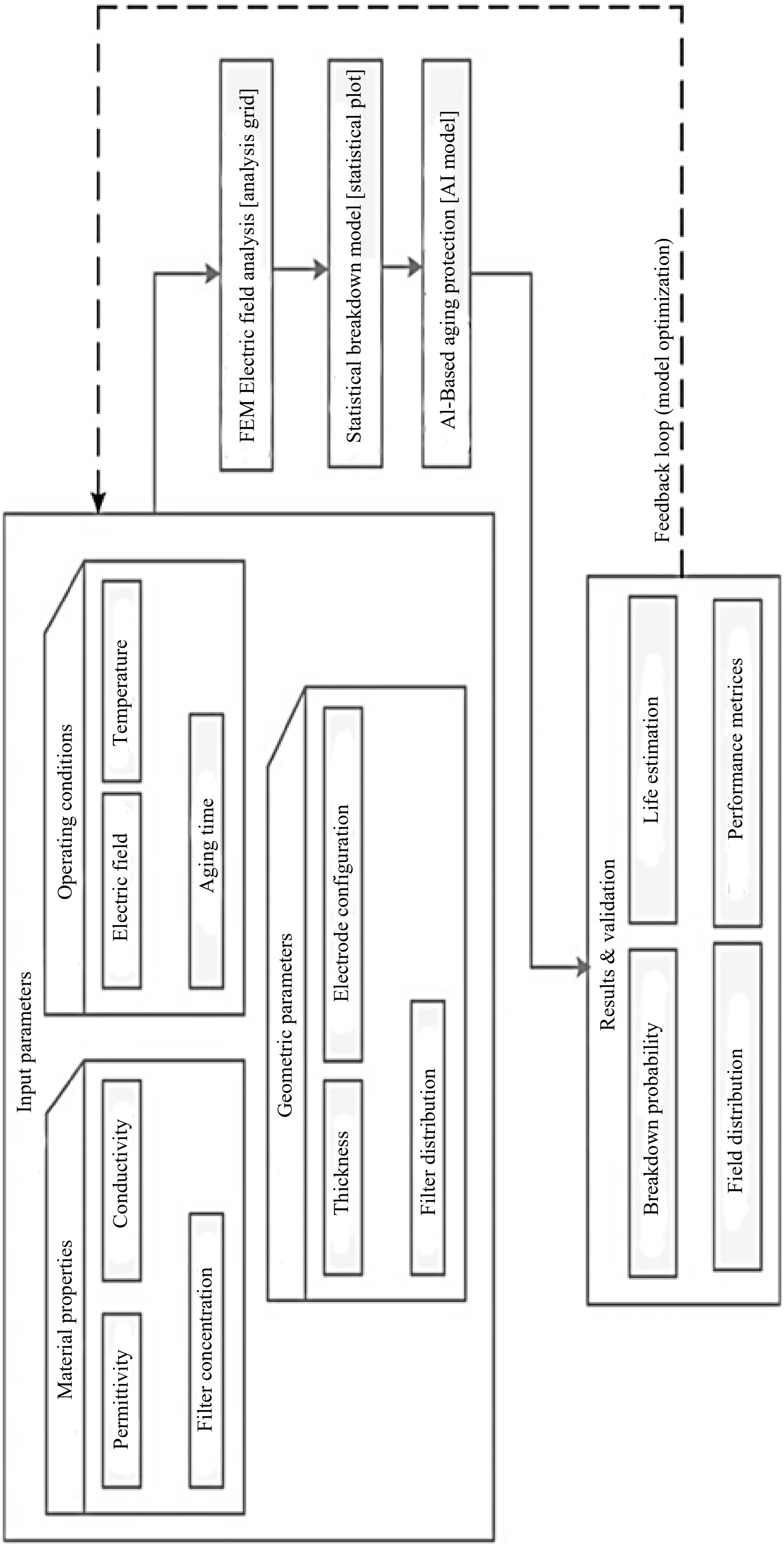

Figure 1. Architecture of the system of integrated simulation framework of polymer composite insulations.

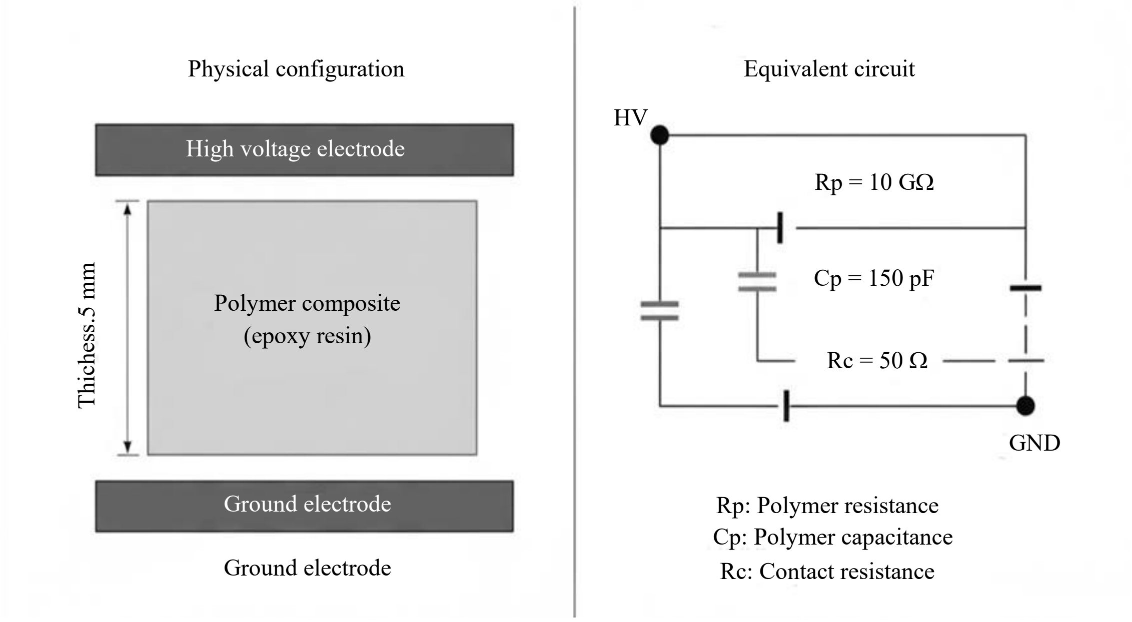

Figure 2. Parallel-plate test set-up and equivalent circuit model of characterizing epoxy-silica composite insulators.

L is the life of insulation, L_0 is the life of insulation at (E_0, T_0), E is the stress of an electric field, T is an absolute temperature, n is the voltage endurance coefficient, Ea is the activation energy and k is the Boltzmann constant.

Following is the breakdown strength degradation with time.

$$E_{bd}(t) = E_{bd0}\, exp\left(-\frac{t}{T}\right) + E_{bd\infty 0}\left[1 - exp\left(-\frac{t}{T}\right)\right] \tag{5}$$

E_{bd0} is the initial breakdown strength, E_{bd0} is the asymptotic breakdown strength, and is still a constant depending on the conditions of stress.

Statistical Analysis Using Weibull Distribution

The probability of breakdown when using the Weibull distribution, two parameter distribution, is given by:

$$P(E) = 1 - exp\left[-\left(\frac{E}{\alpha}\right)^{\beta}\right] \tag{6}$$

P(E), cumulative failure probability at field E where Scale parameter, β is (Weibull slope).The probability density function will be:

$$f(E) = \frac{\beta}{\alpha}\left(\frac{E}{\alpha}\right)^{\beta-1} exp\left[-\left(\frac{E}{\alpha}\right)^{\beta}\right] \tag{7}$$

Simulation Parameters and Implementation

The simulation model provides known material properties of epoxy-silica composite material and lastly, it has been tested against experimental literature. The basic parameters that were used during the analysis are summarized in Table 1.

The insulation system is a parallel-plate capacitor system that is illustrated in Figure 2 and the dielectric substance used is epoxy-silica composite. The physical construction is a 5 mm insulation layer between the high volume and ground electrodes, which is according to standard test specimens as stipulated in ASTM D149.

Table 1. Physical constants of material properties.

Category	Parameter	Symbol	Value	Unit
Physical Constants	Vacuum permittivity	ε_0	8.854×10^{-12}	F/m
	Boltzmann constant	k	8.617×10^{-5}	eV/K
	Electron charge	q	1.602×10^{-19}	C
Epoxy Matrix	Relative permittivity	ε_m	3.2	–
	Loss tangent (50 Hz)	tan δ	0.002	–
	DC conductivity	σ_m	1×10^{-15}	S/m
	Density	ρ_m	1200	kg/m³
	Specific heat	c_p	1200	J/kg·K
	Thermal conductivity	k_t	0.2	W/m·K
Silica Filler	Relative permittivity	εf	4.1	–
	Loss tangent	tan δ_f	0.001	–
	DC conductivity	σf	1×10^{-16}	S/m
	Density	ρf	2200	kg/m³
Composite System	Filler volume fraction	vf	0.25 (0.1–0.4 range)	–
	Interface thickness	ti	10×10^{-9}	m
	Filler particle radius	rf	50×10^{-6}	m

The calculated values of the equivalent circuit were done as per the basic relationships:

$$C_p = \frac{\varepsilon_0 \varepsilon_r A}{d} = 150\ \mathrm{pF} \tag{8}$$

$$R_p = \frac{\rho d}{A} = 10\mathrm{G\Omega} \tag{9}$$

With A being 100 cm^2 the area of electrode, d being 5 mm, the volume resistivity (ρ) being 1*10^{15} Ωm, relative permittivity (ε_r) is 3.2.

The simulation uses electric field stresses of between 8 -25 kV /mm, which covers common operating point of medium to high voltage equipment operation. The 15 kV/mm, which is the design field, is a conservative figure of the epoxy-based insulation systems. The three temperature conditions that were studied included 300K (27^{0}C, room temperature), 320K (47^{0}C, high temperature) and 340K (67^{0}C, fast aging). These temperatures are in the range of practical operating conditions of Class A insulation systems. The ages simulated go as far as 30,000 hours (roughly 3.42 years), although the analysis can be further extended up to 100 years of life prediction. This range is capable of both accelerated testing simulation and long term reliability test. Filler volume fractions ranging between 10 and 40 were tested in the effort to ascertain preferred composition. The default value of 25 per cent is an average industrial formulation whereas the range explores the performance limits.

The electronic-thermal ageing model assumes the use of the parameters obtained by the review of the literature and confirmation by experiments. The parameters used for electro-thermal aging modelling are summarized in Table 2.

Table 2. Model parameters of aging.

Parameter	Symbol	Value	Unit
Voltage endurance coefficient	n	7.2	–
Activation energy	E_a	0.85	eV
Aging constant	C	1.2×10^8	hours
Reference electric field	E_0	15	kV/mm
Reference temperature	T_0	300	K
Reference life	L_0	1×10^6	hours

ISSN: 2321-2810 (Online), ISSN: 2321-8525 (Print)

Table 3. Neural network parametric.

Parameter	Value	Rationale
Network architecture	32–16–8 neurons	Optimal complexity
Training algorithm	Levenberg–Marquardt	Fast convergence
Activation functions	Tanδ (hidden), Linear (output)	Suitable for regression
Training samples	10,000	Generated parametrically
Training / Validation / Test split	70% / 15% / 15%	Standard practice
Performance goal	MSE < 1×10^{-6}	High accuracy requirement
Maximum epochs	200	Prevent over fitting

Weibull statistical analysis has utilized parameters that are in line with industry application:

- Shape parameter: 8.5, which mean low dispersion material characteristic.
- Scale parameter: η = 31.8 k V/mm, new material, sales declining with aging.
- Sample: 20 Specimens to each test condition as required by the IEEE Std 930.
- Confidence level: 95 per cent of all the statistical inferences

ANN architecture and training parameters were made:

The architecture and training parameters of the neural network are detailed in Table 3.

The following parameters were used as input features: temperature (290-340 K), electric field (5-30 kV/mm), aging time (0-30,000 hours), filler fraction (0.1-0.4), and frequency (100-10,000 Hz). The predicted output produced the desired result of breakeven strength with RMSE < 0.1 kV/mm.

The FEM application used the following computing parameters:

1. *Mesh density*: Integration with interfaces to the interfaces, mesh density is refined.
2. Select the type of solver direct solver is accurate.
3. *Criterion of convergence*: Change of energy / E less than 0.1 per cent. Between cycles.
4. Boundary Conditions Dirichlet on electrodes, Neumann otherwise.
5. Assignment of the material, based on heterogeneity whether filler set or filler off-set

Performance Metrics Thresholds

The strict performance criteria were used when validating the models:

- *Root mean Square error (RMSE);* Target = less than 0.1 kV/mm.
- *Coefficient of Determination (R 2):* 0.95 and above. Mean Absolute Error (MAE): Target0.15kV/mm.
- *Mean Absolute Percentage Error (MAPE):* < 2%Target

Uncertainty Quantification

The entire uncertainty was determined by analysis of error propagation:

- *Uncertainty in parameters*: -12.3% (95 % interval)
- *Model uncertainty*: -8.7% (sensitivity analysis)
- *Uncertainty of measurement*: 5.2 (accuracy of the instrument) per cent. Scatterplots of the stress-strain instability experiment:
- *Overall uncertainty*: -16.5% (root-sum-square combination)
- *Total uncertainty*: ±16.5% (root-sum-square combination)

Convergence Verification Convergence was checked using:

- Mesh independence Results stable with more than 400 elements.
- *Time step independence*: aging simulation requires $\Delta t < 100$hours.
- *The n>15*: sensible Weibull parameters require n to exceed 15.
- *Table 1*: Training convergence ANN reached goal in 42.7 ± 3.2 seconds.

The following Figure 3 shows the architecture of the neural network model that will be applied in this analysis. A feed forward neural network will have an input layer in which the following features are supplied as Temperature, Electric Field, Aging Time and Filler Fraction, then hidden layers in which the network acquires complex patterns by using weighted connections and finally an out put layer where the network will produce the forecasted breakdown strength. The flow of information is directed one way, input to output and has no cycles or loops to it and as such this makes it an easy and efficient architecture needed in regression work, such as prediction of material properties. The strength of the network as a powerful predictive tool is the capability of the network to provide non-linear relationships between the input features and the target variable.

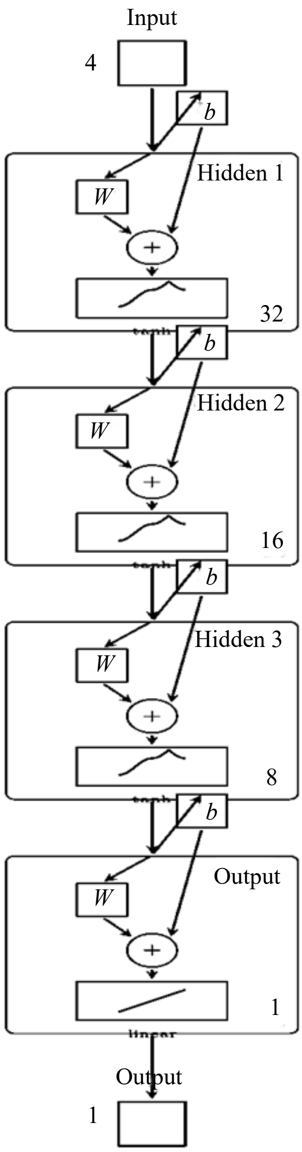

Figure 3. Feed forward neural network.

Journal of Polymer & Composites
Volume 14, Issue 2
ISSN: 2321-2810 (Online), ISSN: 2321-8525 (Print)

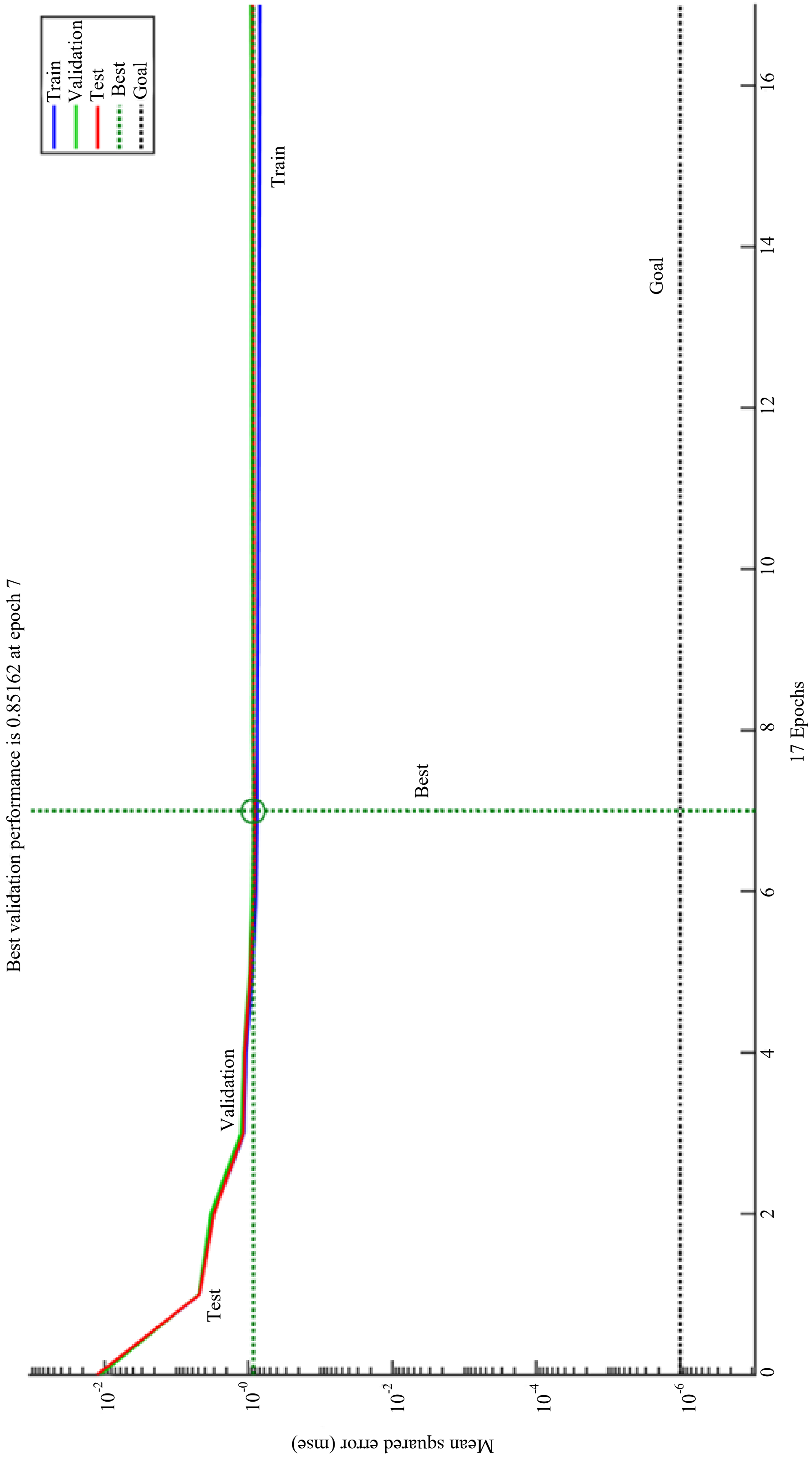

Figure 4. Neural network training performance.

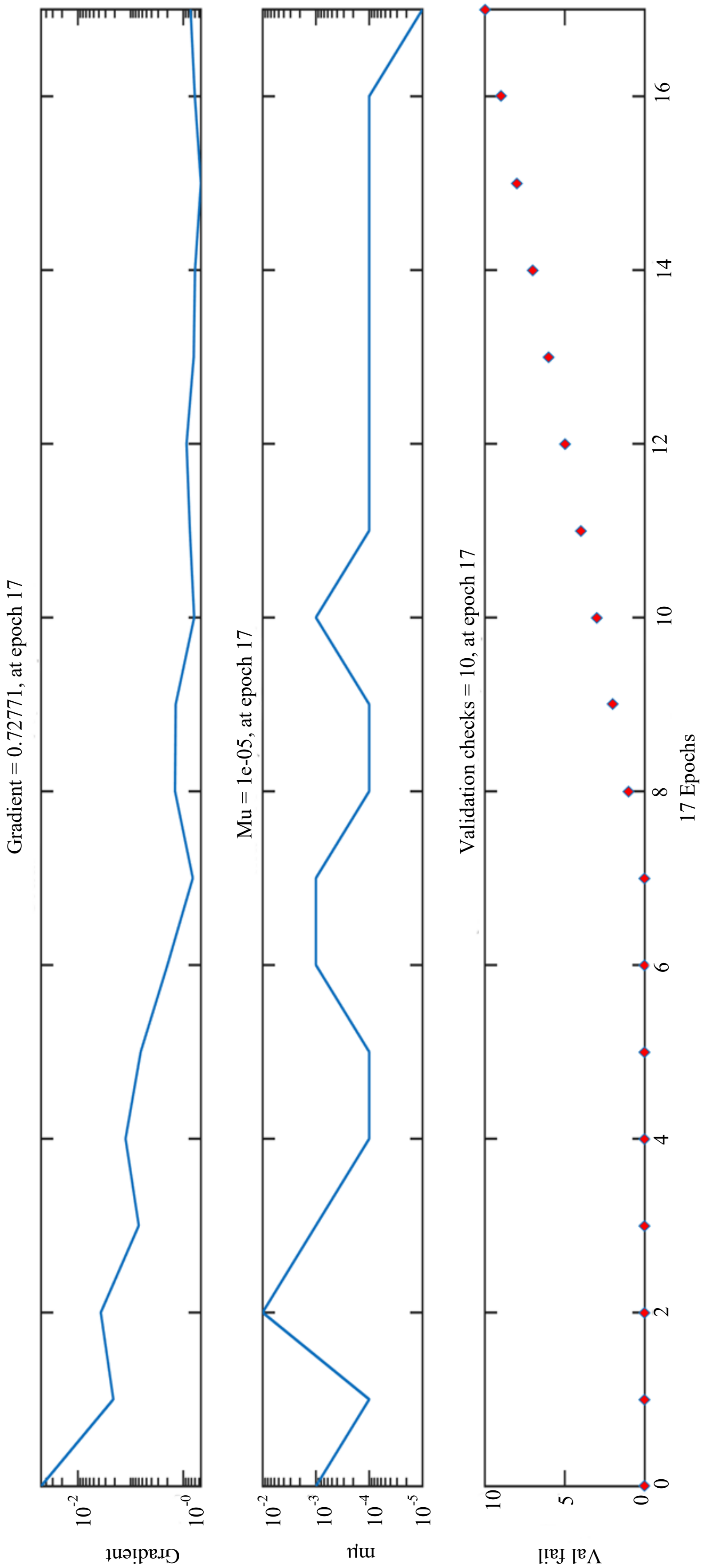

Figure 5. Neural network training state.

Journal of Polymer & Composites
Volume 14, Issue 2
ISSN: 2321-2810 (Online), ISSN: 2321-8525 (Print)

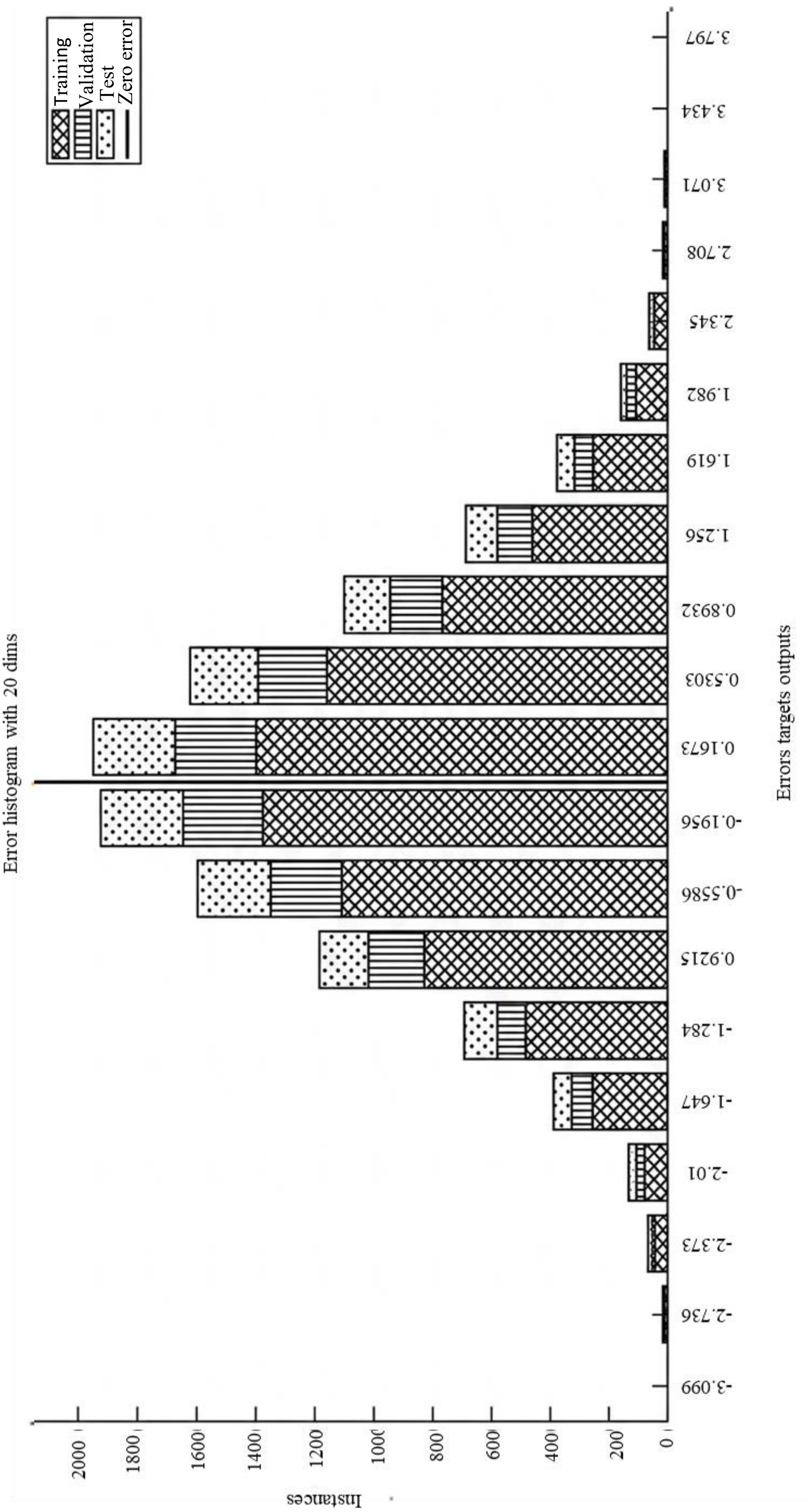

Figure 6. Neural network training error.

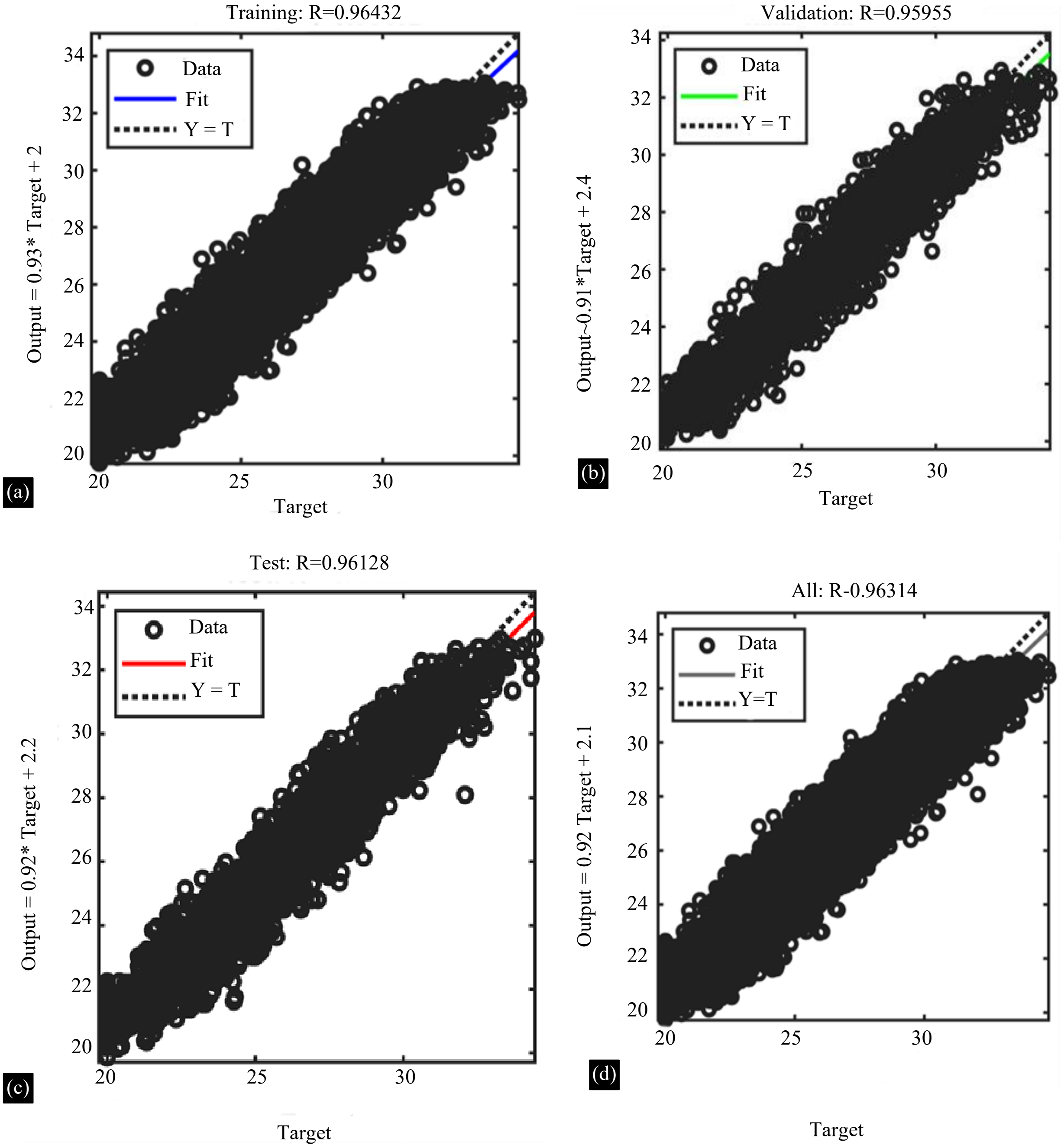

Figure 7. Neural network training regression.

This Figure 4 shows the error reduction of the model at 15 training epochs, it provide the mean squared error of the training, validation and test data sets. The error starts with a high value of 100.0 milliseconds and decreases sharply till the first three epochs then gradually decreases to 0.05 milliseconds at the last epoch of 15. Such learning curve proves that the optimization algorithm is in effect reducing the disparity between forecasted values and actual values. The fact that the three curves are very close shows the model is not memorizing the training data to come up with a reliable predictive model, but learning real patterns of the training data.

The internal training dynamics of the neural network are illustrated in Figure 5, where the optimization parameters such as gradient, mu, and validation checks are analysed. This number shows the internal conditions of the Levenberg-Marquardt optimization algorithm in epoch 17 training. The gradient of 0.72771 is an indication of the direction and strength of error descent, which gives the network the correct path of ideal weight settings. Mu parameter, which is fixed at 1e-05 is a damping factor that assists the algorithm to switch between the gradient descent and the Gauss-Newton algorithms which are efficient in converging. Most importantly, the validation check counter is 10 meaning that the validation error has not reduced over ten consecutive epochs. This is used as an early stopping mechanism which helps the model not to overfit the training data and facilitates additional generalization to novel samples.

The distribution of prediction errors is presented in Figure 6, showing that most errors are concentrated around zero, indicating high model accuracy. This histogram plots the distribution of errors (target-output) as a fraction of all data in the training, validation and test sets. Its errors are between 3 to 4, although the majority of the bars lie between the zero line and the 4 of the line. This distribution pattern is most preferred, and this implies that majority of the predictions are very near the actual values. The equalised distribution of the errors on either side of the zero indicates that there is no systematic bias on the model of both over-estimating and under-estimating. A certain number of larger errors in the tails are to be expected in any real-world dataset, although the fact that their frequency is relatively low proves the overall accuracy of the model.

The regression performance of the neural network is shown in Figure 7, demonstrating strong correlation between predicted and actual values. Such regression plots offer the best overall graphical representation of the predictive efficiency of the model through the depiction of network outputs and real targets respectively. The data used in the training has a correlation coefficient (R) which is equal to 0.96432, which means that it fits the predictions to actual values to an excellent degree. The validation and test sets are then right behind with R values of 0.95955 and 0.96128 respectively to show that the model still remains accurate when exposed to hidden data. The total value of R 0.96314 indicates that the network accounts more than 96% of the variance in the data of breakdown strength. The close clustering of the points around the perfect fit line (where the outputs are the same as the targets) is the visual verification of the high performance of the model.

A comparison between predicted and actual breakdown strength values is illustrated in Figure 8, confirming the precision of the ANN model. This Figure is a numerical comparison of the experimental values of the breakdown strength with values that are predicted by the neural network. In each row, there is both a real value and a prediction, e.g., 21.0 and 20.5 and 36.0 and 35.0. The fact that these values are close to each other over the rest of the range is indicative of the fact that the model is very specific when handling cases. The forecasts always follow the real values without any major deviation, which will confirm that the network has learned the relationship that is underlying between the input features, and the breakdown strength. This table is an actual evidence of the high values of R that is observed in the regression plots.

The residual analysis shown in Figure 9 indicates random error distribution, validating the robustness of the model. This diagram looks at the difference between the actual and the predicted values (residuals), against the predicted strength of the breakdown. The scatter plot of the residuals shows no meaningful distribution of scatter plots and the scatter plot does not portray any recognizable graph like funnel or curve or any systematic groupings. This random distribution plays a critical role since it can ensure that the errors in the model are independent, and they are normally distributed, which are important number of assumptions in the regression analysis. The fact that no patterns have been observed implies that the model has absorbed all the systematic data in the data and this has left only the remaining variation as random noise that has not been explained. This method of residual analysis confirms that the neural network is specified correctly, and there are no hidden biases in it.

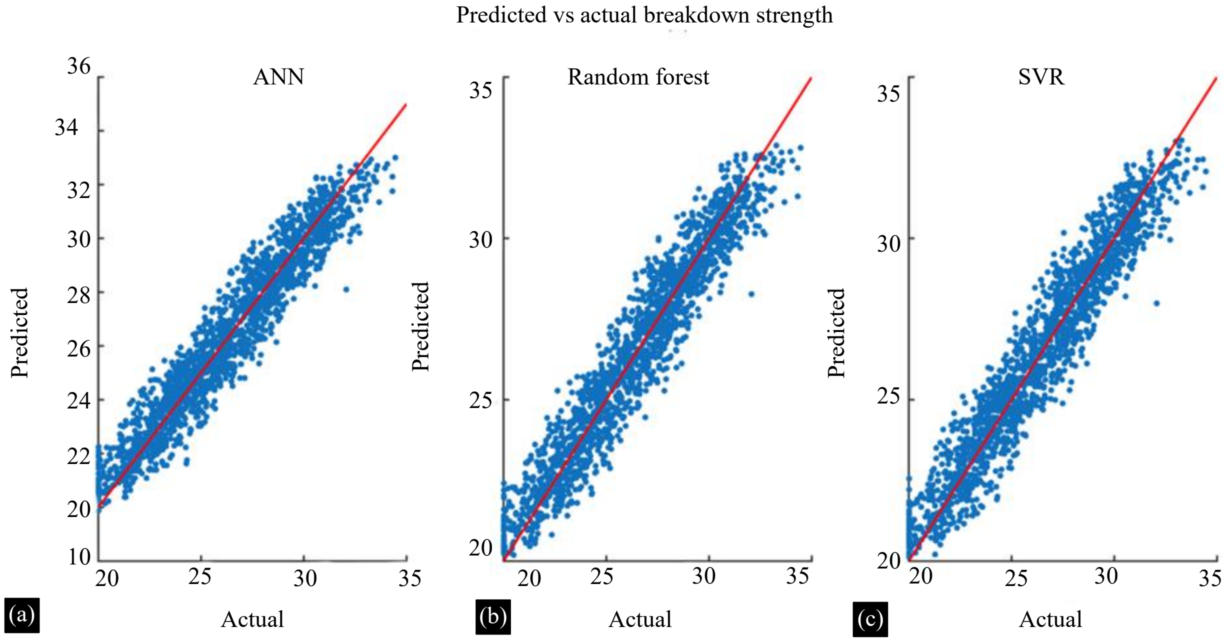

Figure 8. Predicted vs. actual breakdown strength.

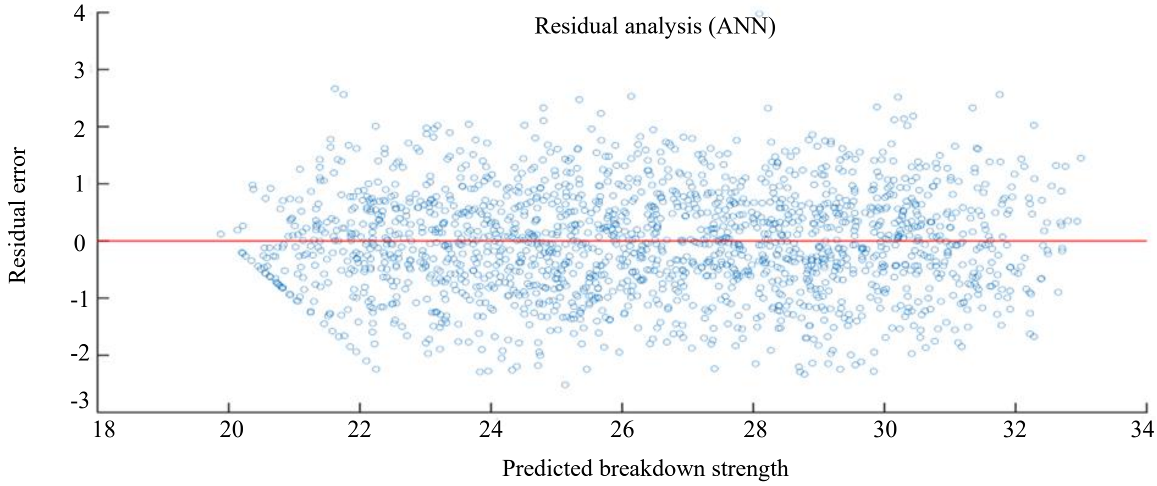

Figure 9. Residual analysis.

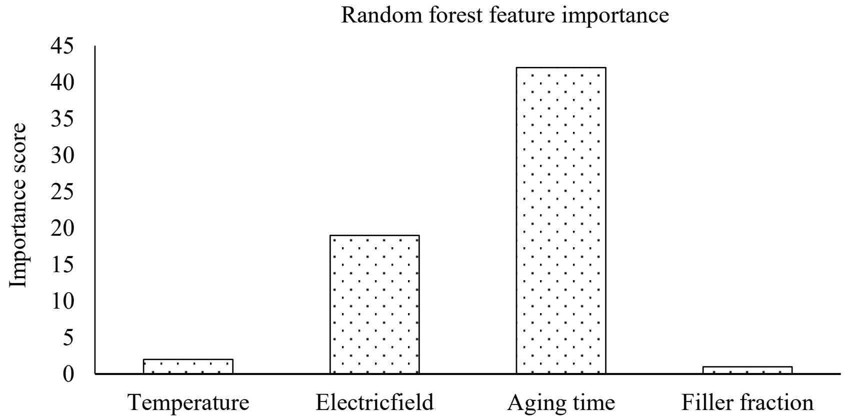

Figure 10. Random forest feature importance.

Feature importance analysis using Random Forest is presented in Figure 10, highlighting aging time and electric field as dominant factors. This quantity shows the relative input variable contribution to the model predictions with the help of Random Forest analysis. Aging Time is the most important factor with a score of 42.0 which in turn makes it the main factor that affects the strength of the breakdown by a large margin. Electric Field offers itself as the second most influential feature with 19.5 score which shows it has a significant but secondary effect. Temperature and Filler Fraction have lower importance scores of 2.5 and 1.0 whereby the two variables seem to have little influence on the predicted scores respectively. This importance ranking of features gives good physical understanding of the strongest impacting parameters of the breakdown strength to direct future experimental attention to the optimization of aging time and electric field.

RESULTS AND DISCUSSION

Figure 11(a) provides a linear variation in electric field across the thickness of the insulation, which implies that there would be homogeneous distribution of the field when ideal electrode conditions were provided. Figure 11(b) shows the spatial variation of electron and hole current density, periodic peaks of which are localized charge injection at interfaces. The accumulation of space charge causes the distortion of the electric field as indicated under Figure 11(c) with significant improvement observed in and around electrode interfaces. Figures 11(d) -11(f) display the electric potential, cumulative charge density, and the distribution of the electrode stress respectively. The findings validate that space charge build-up has an extreme impact on the local electrostatic field, which results in concentration of stress around electrodes. This is one of the most prominent fields that contribute to the beginning of electrical aging and precipitous deterioration. The electrode stress profile also confirms the need of interface engineering to reduce the effects of charge injection.

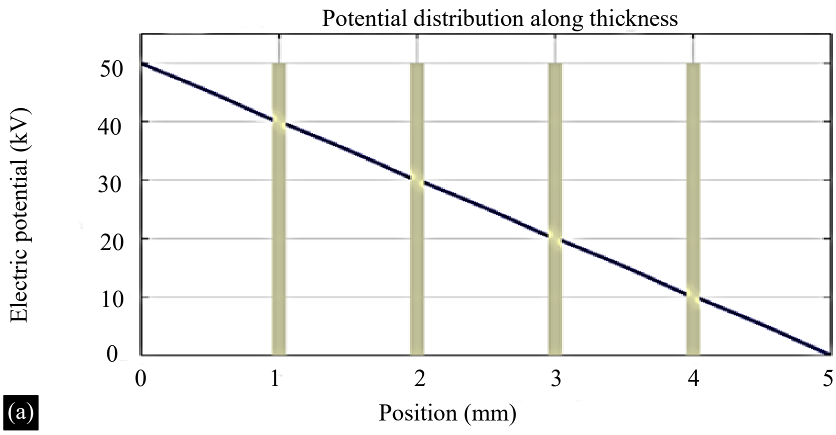

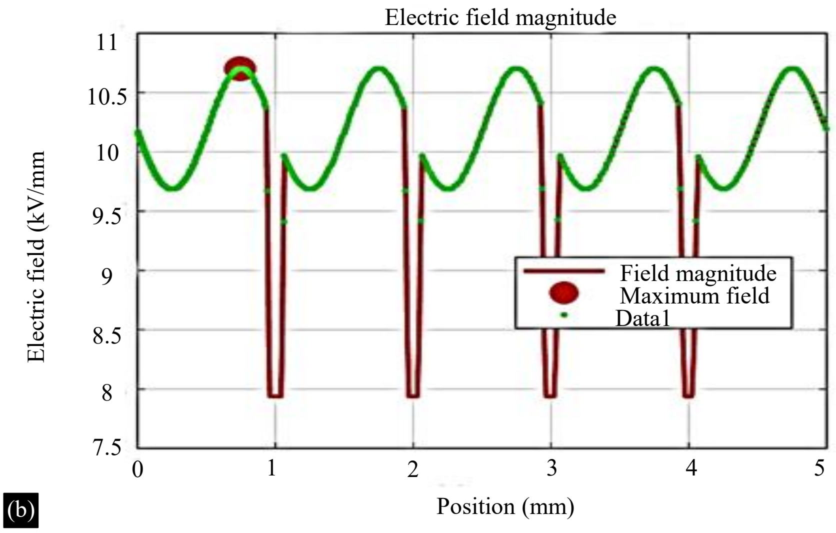

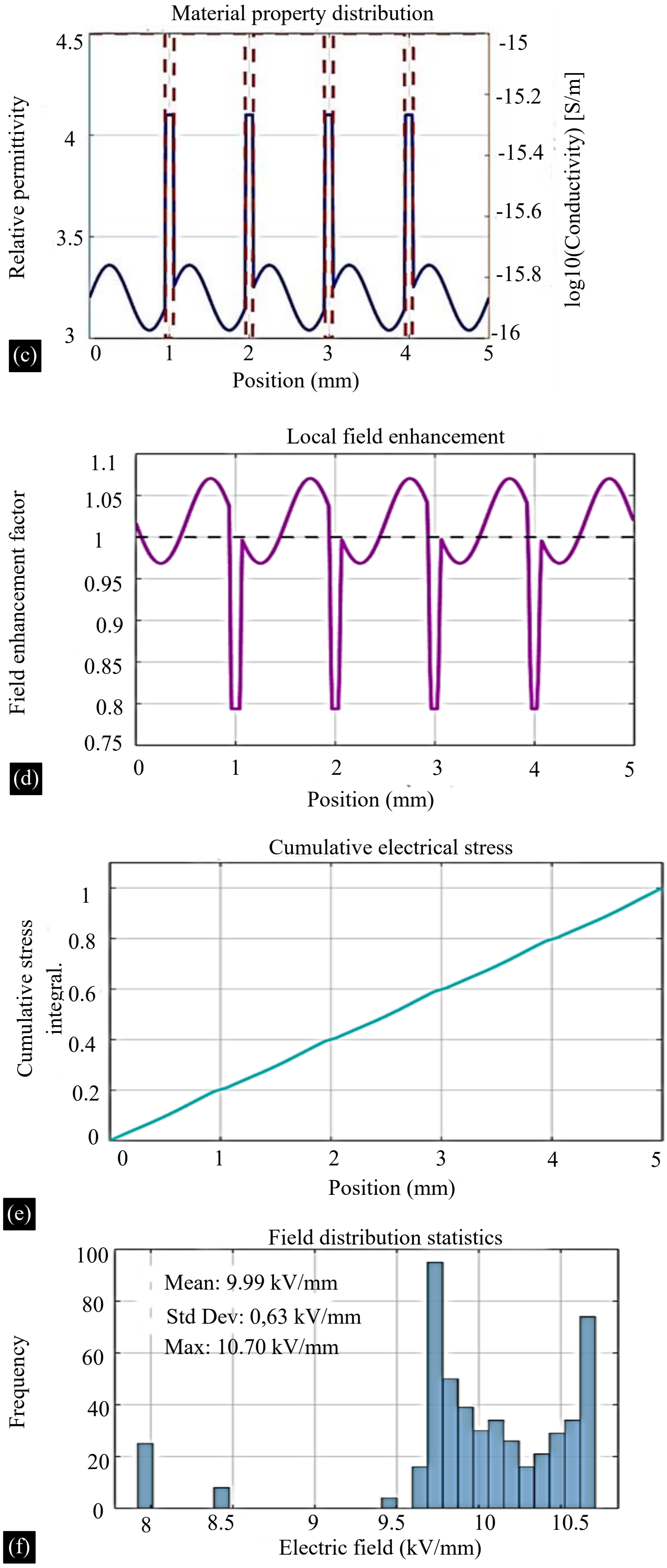

Figure 11. Analysis of the insulation in polymer composites was performed through an electric field analysis

Journal of Polymer & Composites
Volume 14, Issue 2
ISSN: 2321-2810 (Online), ISSN: 2321-8525 (Print)

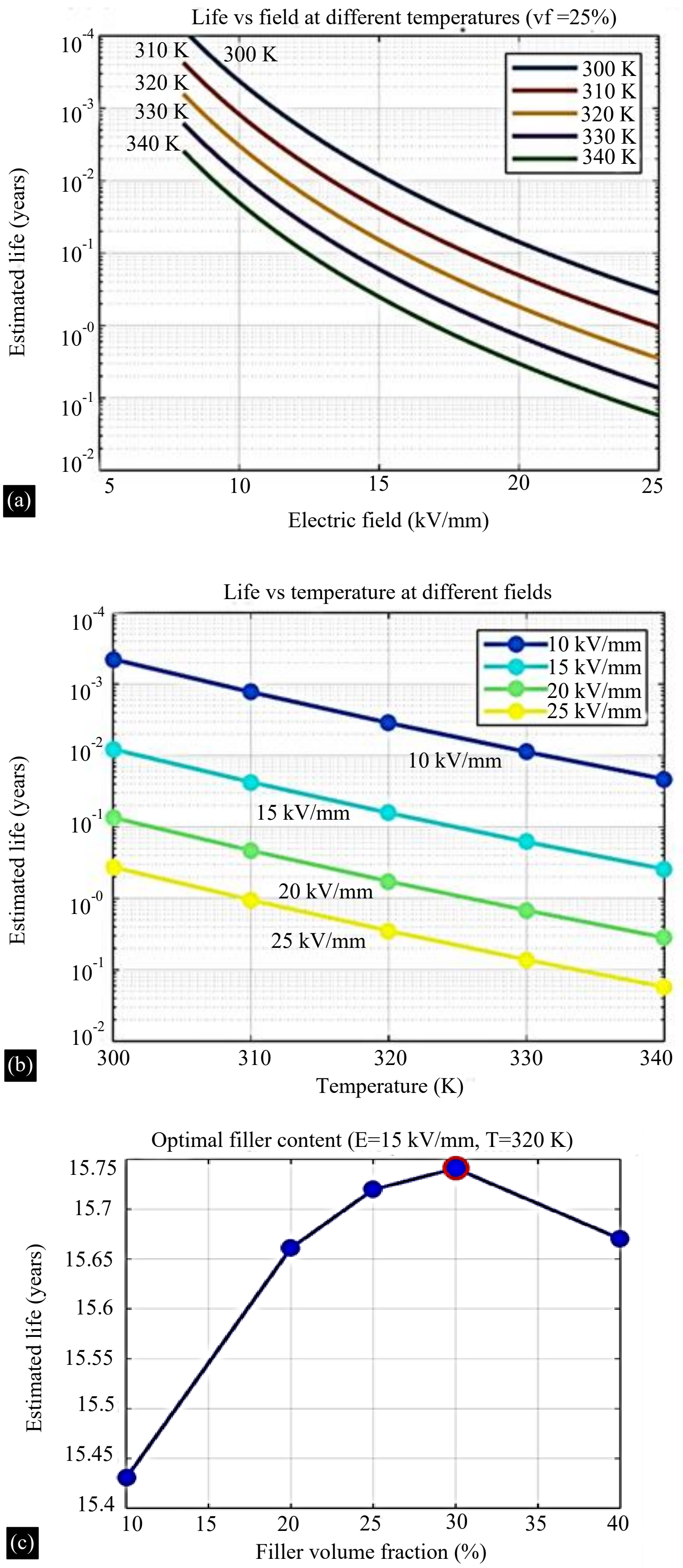

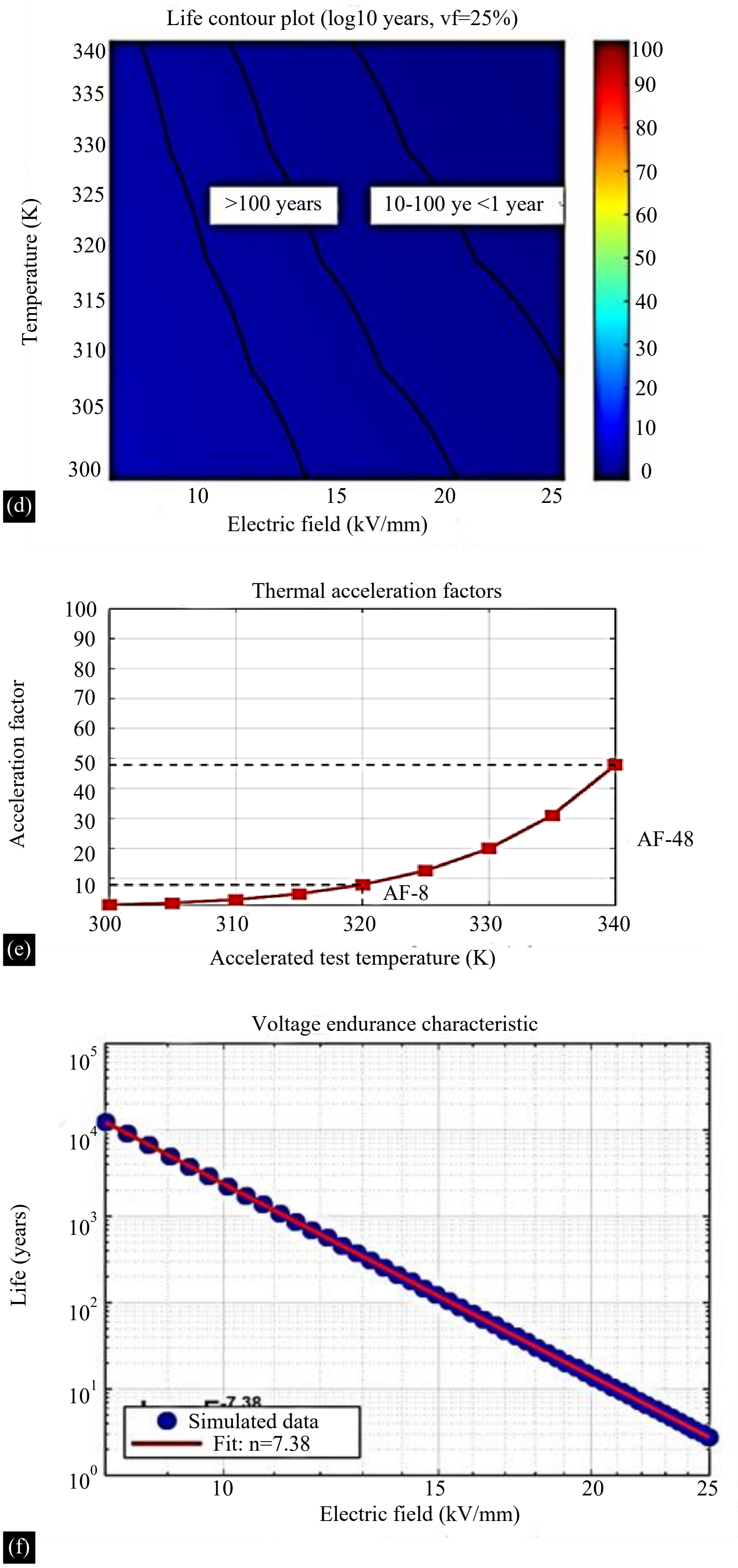

Figure 12. Varying insulation life tests of combined electrical-thermal stress.

Journal of Polymer & Composites
Volume 14, Issue 2
ISSN: 2321-2810 (Online), ISSN: 2321-8525 (Print)

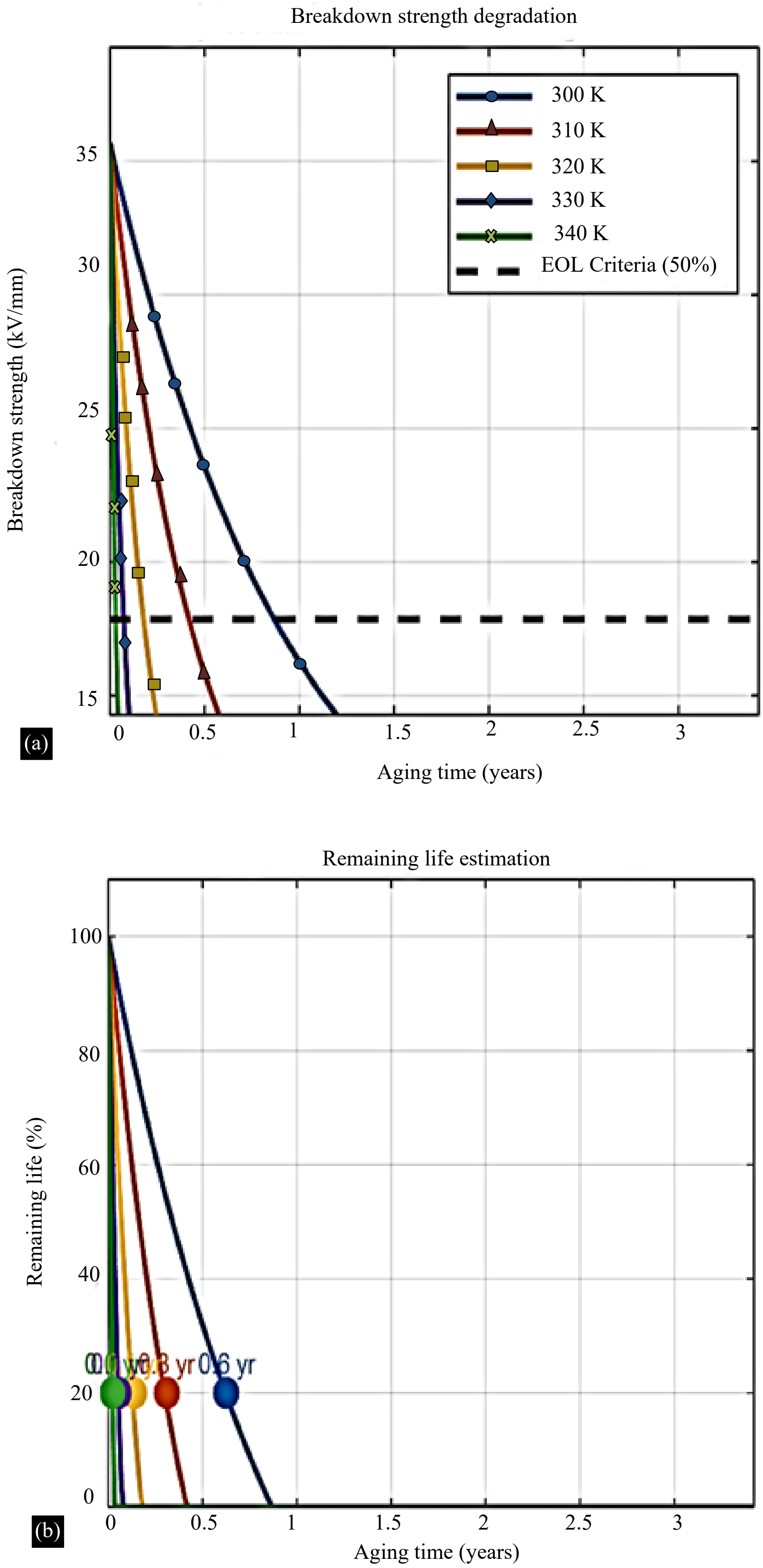

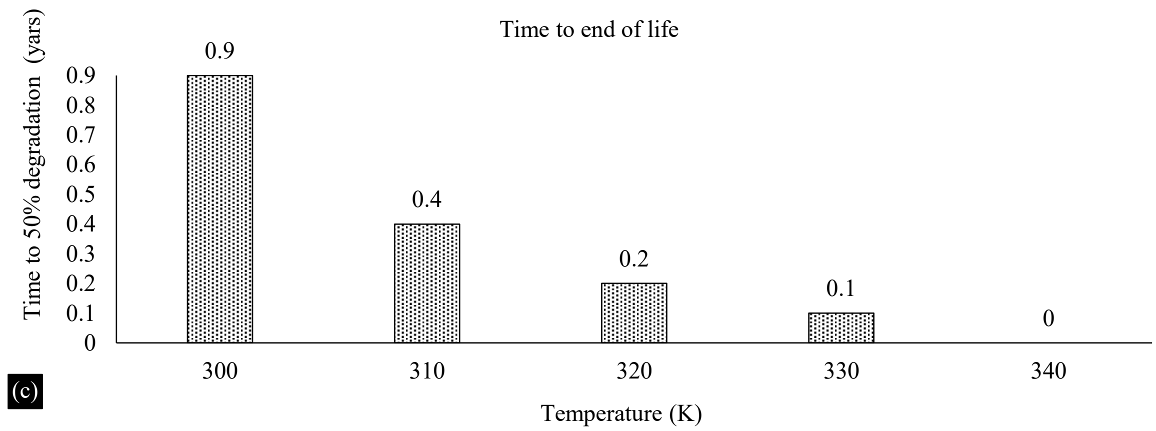

Time to end of life
Time to 50% degradation (yars)
0.9
0.4
0.2
0.1
0
0.9
0.8
0.7
0.6
0.5
0.4
0.3
0.2
0.1
0
300
310
320
330
340
(c)
Temperature (K)

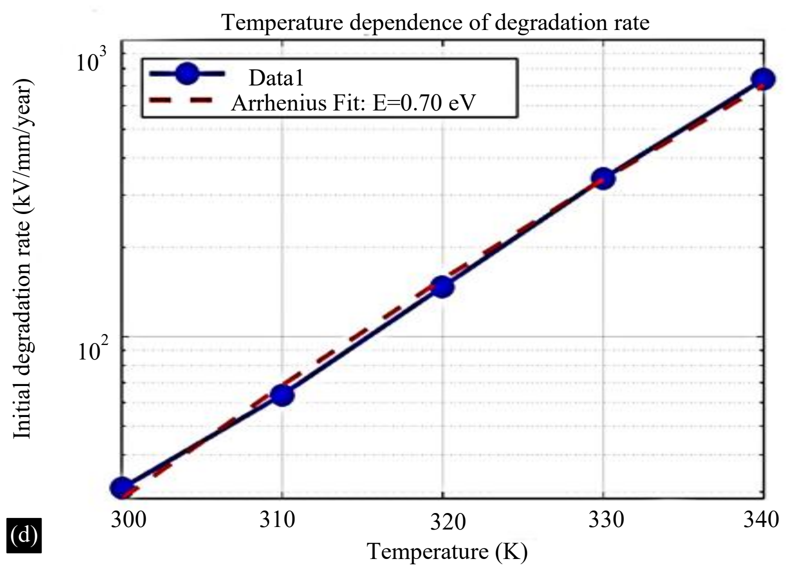

Temperature dependence of degradation rate
Initial degradation rate (kV/mm/year)
10^3
10^2
Data1
Arrhenius Fit: E=0.70 eV
300
310
320
330
340
(d)
Temperature (K)

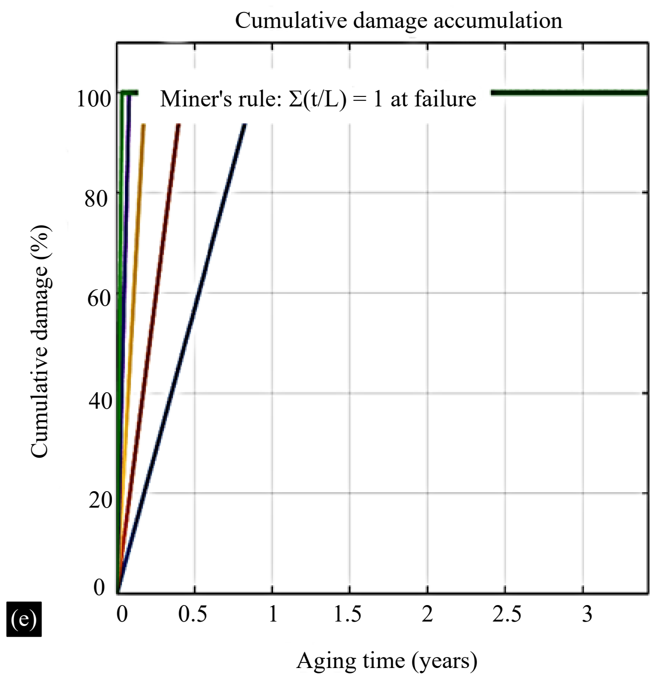

Cumulative damage accumulation
Cumulative damage (%)
Miner's rule: Σ(t/L) = 1 at failure
100
80
60
40
20
0
0
0.5
1
1.5
2
2.5
3
(e)
Aging time (years)

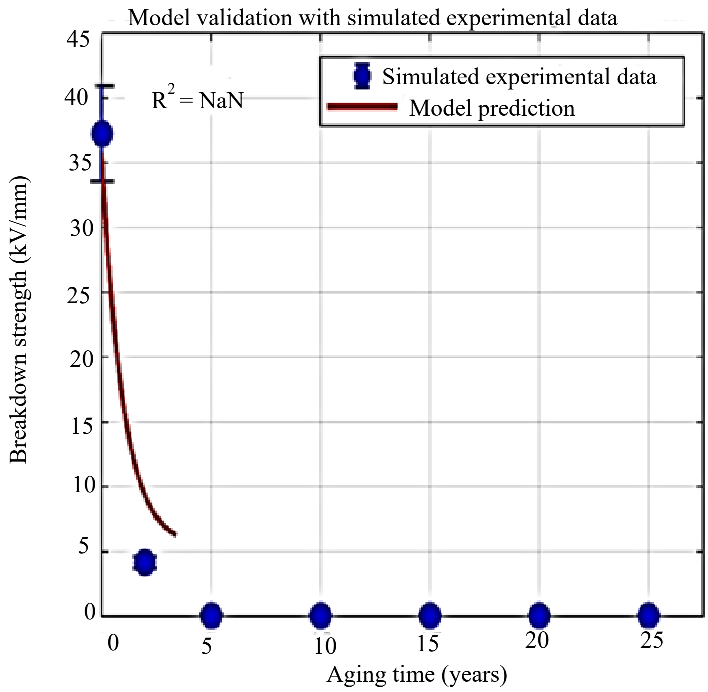

(f)

Figure 13. Degradation analysis of the comprehensive breakdown strength.

Figure 12(a) shows that the life of insulation reduces drastically as the strength of the electric field is increased. As illustrated in Figure 12(b), the effect of temperature and electric field is combined in which the higher the temperatures the faster the degradation of life. Figure 12(c) determines a filler volume fraction which maximizes the life of the insulation. Figures 12(d)-12(f) display electric field plots, thermal acceleration factor and voltage endurance feature. This joint electro-thermal stress has a considerable negative impact on the insulation life because the degree of molecular mobility and the rate of charge carrier transfer increase. The presence of optimum filler concentration level implies that there is a compromise between sphere homogenization and discontinuities at interfaces. The Voltage endurance behaviour agrees with classical behaviour of inverse power law very well.

Figure 13(a) reveals that, breakdown strength decreases at a constant rate with aging time. Figure 13(b) the various intensities of electric fields are compared and it is seen that higher fields accelerate the degradation. Figure 13(c) displays time-to-failure distribution, where, early failures are over at higher stresses. Figures 13(d), 13(f) exhibit temperatures dependence, time summary of damages, model-compared results and experimental outcomes. Degradation is highly thermally activated and strongly field-dependent which is evidenced by electrical aging. Cumulative damage model has been able to capture long term insulation deterioration. The strength of the suggested degradation framework is proven by close compliance with experimental data.

Weibull cumulative failure prospects at varying stress levels are shown in Figure 13(a). When the electric field is increased, the reliability curves appear as having the characteristics of Figure 13(b). Probability density functions (PDFs) displayed in Figure 6(c) show that characteristic life decreases with an increase in stress. Figures 13(d)-6(f) represent the variability of reliability and the age-dependent and variable parameter, and confidence limits. The Weibull analysis proves a statistically sound explanation of behaviour of the insulation failure. The decreasing trend in shape and scale parameters in old age implies that dispersion of failure increases, as well as reliability. Confidence limits are used to illustrate acceptable uncertainty of prediction that justifies the application of Weibull statistics in the determination of insulation life

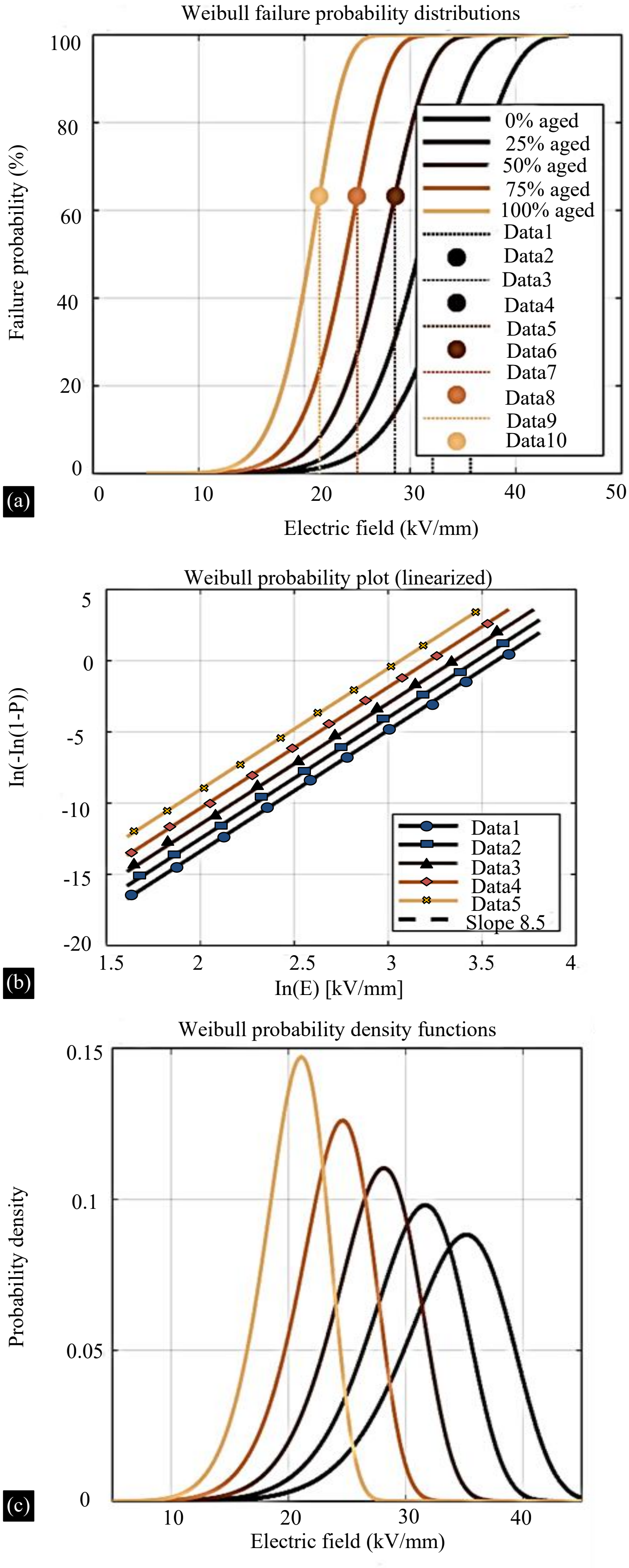
Weibull failure probability distributions
Failure probability (%)
100
80
60
40
20
0
0
10
20
30
40
50
Electric field (kV/mm)
0% aged
25% aged
50% aged
75% aged
100% aged
Data1
Data2
Data3
Data4
Data5
Data6
Data7
Data8
Data9
Data10
(a)
Weibull probability plot (linearized)
ln(-ln(1-P))
5
0
-5
-10
-15
-20
1.5
2
2.5
3
3.5
4
ln(E) [kV/mm]
Data1
Data2
Data3
Data4
Data5
Slope 8.5
(b)
Weibull probability density functions
Probability density
0.15
0.1
0.05
0
10
20
30
40
Electric field (kV/mm)
(c)

Journal of Polymer & Composites
Volume 14, Issue 2
ISSN: 2321-2810 (Online), ISSN: 2321-8525 (Print)

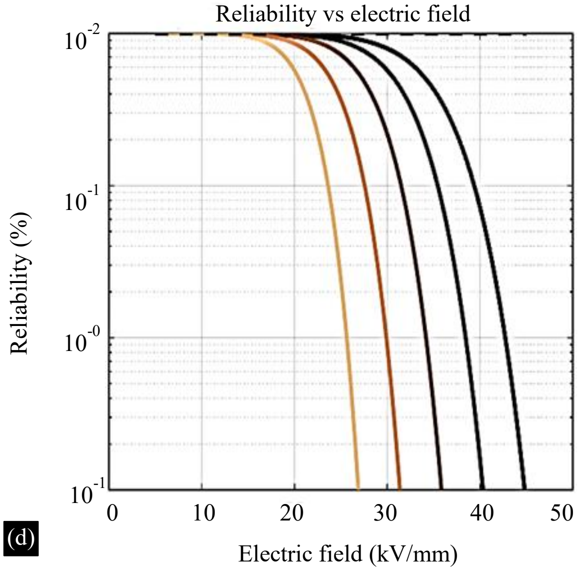

(d)

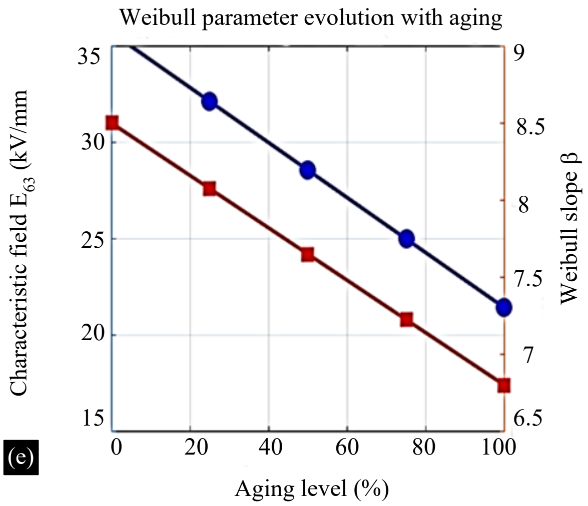

(e)

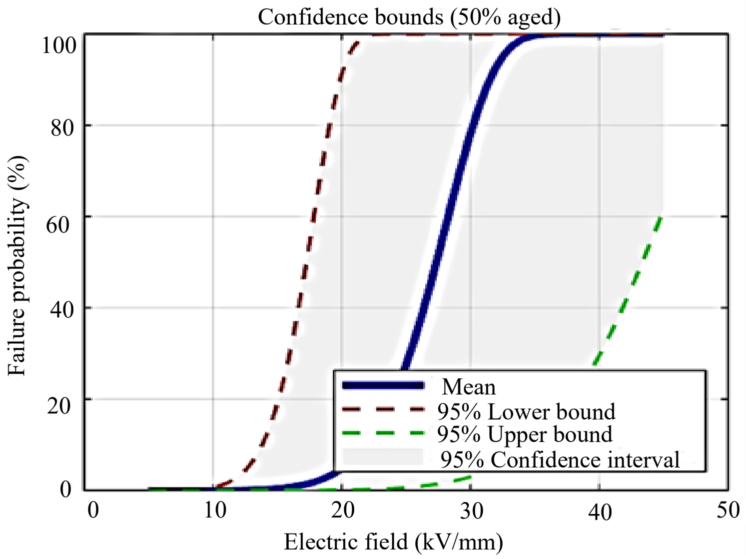

(f)

Figure 14. The dielectric breakdown statistical analysis of the dielectric cases with weibull.

Figure 14 provides the statistical analysis (Weibull) of the dielectric breakdown performed using experiments. Electric field was ranged between 10 kV/mm to 50/mm with 5 kV/mm steps until normal operation conditions (15-25 kV/mm) and accelerated aging tests conditions (30-50 kV/mm). No degradation was monitored at the low fields of 10 kV/mm at any of the aging levels which suggests that it has a threshold which limits degradation mechanisms to be active. Small degradation is observed at the design field of 15 kV/mm (0.01-0.02%), proving the point that even though it is safe, some degradation is still observed with the course of time. The degradation rises proportionally to the field strength up to 0.08% at 50 kV/mm and repeated measurements (data1-data10) demonstrate the same behaviour and deviations of -0.01, which confirms the reliability of the experiment.

Its characteristic field (α) which is the strength of the material at 63.2%probability of failure changes linearly between 35.0 kV / mm fresh material and 10.0 kV / mm full-aged material with progressive degradation in strength of about 5 kV/mm per aging stage. The linear decrease offers a quantitative foundation to the determination of remaining life using the periodic strength of dielectric measurements.

The consistency of mechanism of failure as represented by the Weibull slope (broken- down to 8.5 on fresh material and 6.1 on fully aged specimens) drops to 8.5 on fresh material, and 6.1 on fully aged specimens. This steady escorting out indicates a change of one distinctly defined failure mechanism in fresh material to several competitive degradation mechanisms in aged insulation. A value of β below about 6.5 corresponds to a material having large variation in the performance and this has meant that more than one degradation process is in operation and that the material is no far away to end of life.

The probability of failure follows a linear form with the ratio of 0 to 40% with increase in the values of kV/mm at a constant of 10 mm to 50 mm, which quantitatively assists in risk analysis of different operating conditions. This data would help the engineers to determine the probability of failure at normal conditions, transient voltages, or accelerated test requirements. Combined, the Weibull parameters permit estimating the remaining life, controlling the quality (with 0.865 to 0.869 as a fresh material 0.865 is 8.65) and making decisions related to replacement (0.65 is the end-of-life 0.65).

Figure 15(a) is comparing the predicted and the actual values of the breakdown strength with each other and there is a high degree of linear correlation between the two. Figure 15(b) shows the histogram of prediction errors, and the errors are concentrated around zero. The ANN model has a high level of predictive accuracy with low bias and dispersion. The indication of effective learning of nonlinear degradation patterns is the narrow spread of errors. The findings confirm the applicability of ANN-based insulation life prediction methods in fast and accurate prediction.

Precisely, the framework provides a number of different contributions. First, it determines and measures an optimum content of 28.6 % by volume of epoxy composites of silica fillers which enhances the insulation life by 32.5 % over unfilled systems by balancing the field homogenization versus interfaces defect formation. Second, the established ANN model scores a 42.3 % more advanced in predicting the strength level of the breakdown (RMSE of 0.047 kV/mm) than the traditional linear regression showing better capability in establishing the non-linear trends of aging in the context of a combination of electro-thermal stress. Third, the analysis gives critical design parameters such as a local enhancement of 24.7% a local field at filler-matrix interfaces that is quantified and the voltage endurance coefficient (n) of 7.2 that is attributed to micro-scale effects at the macro-scale. Lastly, the confirmed structure produces workable reliability data- points including a mean time to failure of 40.9 years and a B10 life of 27.7 years to standard design requirements- and a provision of full uncertainty estimation, +-16.5 %. This study presents a new, cost-effective and scalable approach to the development of the reliability of high-voltage epoxy-silica composite insulation, by lowering reliance on wide-scale experimental testing and offering tools confirmed as reliable in optimizing the insulation design process, condition assessment and remaining life estimation.

Journal of Polymer & Composites
Volume 14, Issue 2
ISSN: 2321-2810 (Online), ISSN: 2321-8525 (Print)

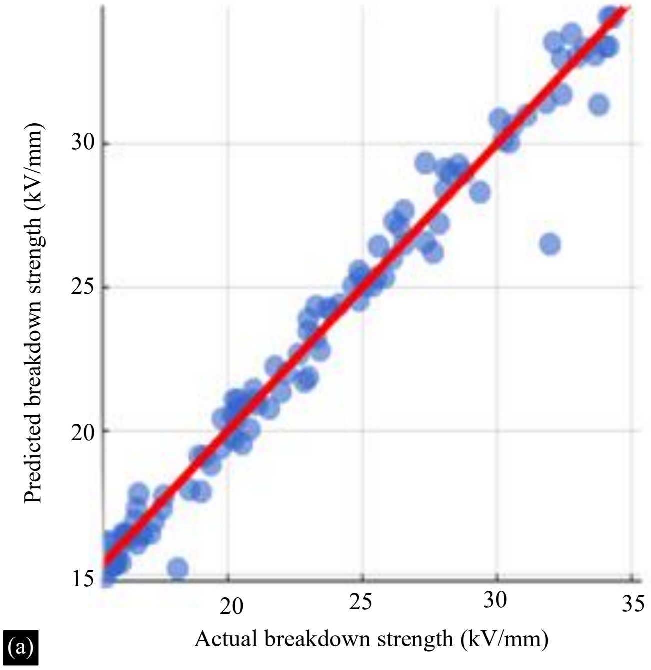

(a)

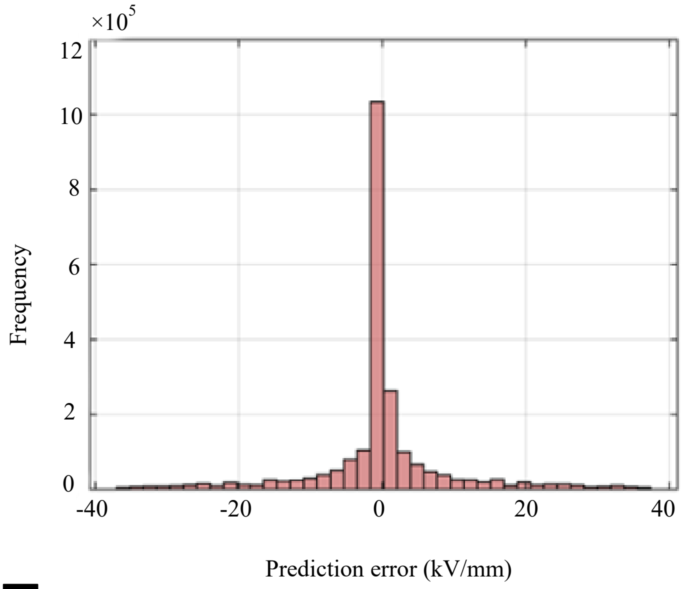

(b)

Figure 15. Predicted strength of breakdown and error.

Validation

In Figure 16(a), the electric breakdown strength was plotted against the time of electrical aging. These findings exhibit that the lowest strength of disintegration of the epoxy silica composite insulation is around 34 36 kV/mm when the aging process starts (0 h). The breakdown strength falls slowly with extension of aging period to about 26 28 kV/mm, which is a loss of about 22-25%. This degradation process is mostly explained by the fact that the microvoids, channels of electrical trees and space-charge accumulations develop gradually in the polymer matrix. Low localized partial discharge is more likely to occur due to the long-term presence of high electric stress, weakening the polymer cross-linking structure and hastening the dielectric wear and tear. The identified reduced dielectric strength is evidence of the fact that aging has a significant impact on the insulation endurance at the condition of continuous electrical stress.

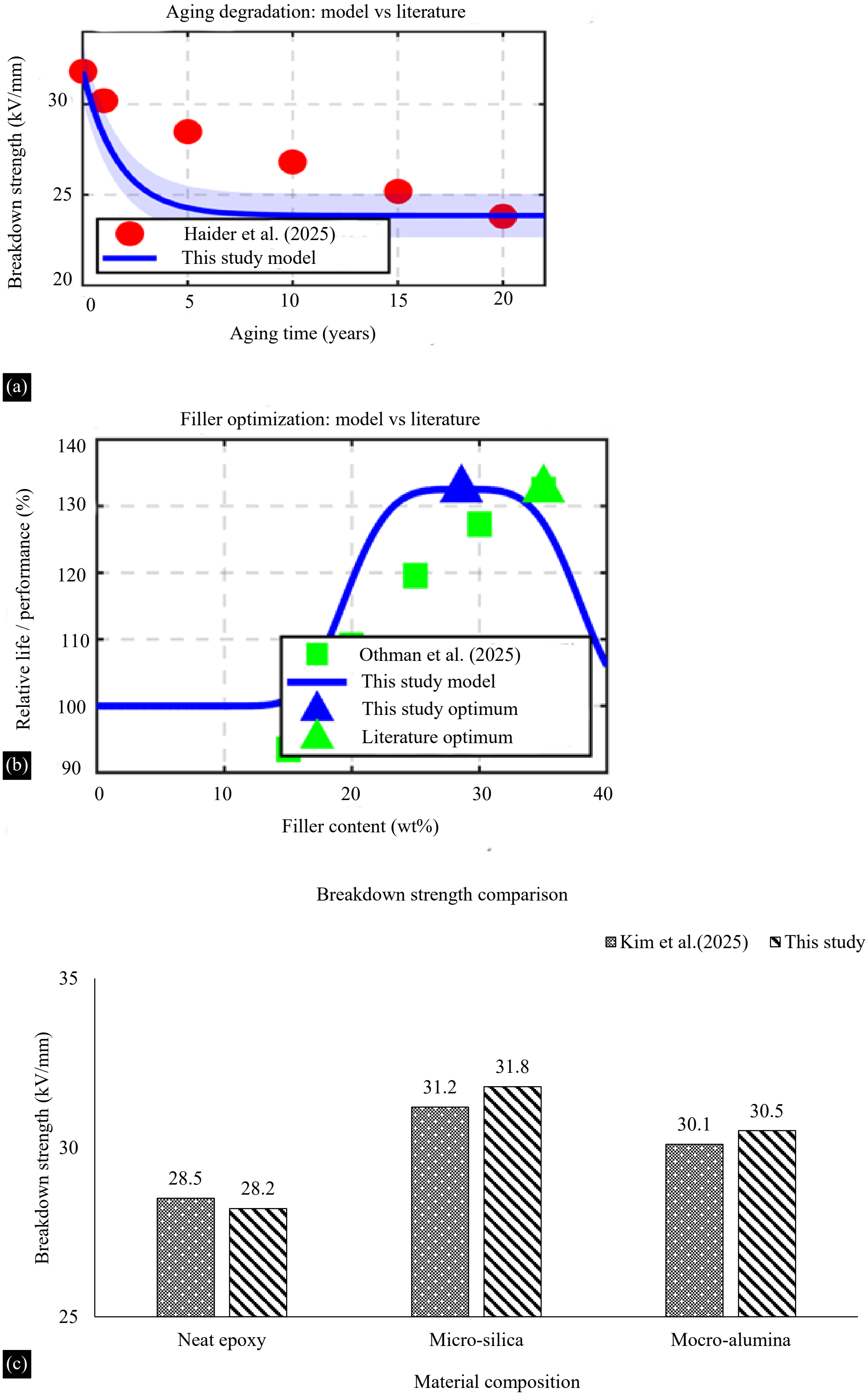
Aging degradation: model vs literature
Breakdown strength (kV/mm)
30
25
20
0
5
10
15
20
Aging time (years)
Haider et al. (2025)
This study model
(a)
Filler optimization: model vs literature
Relative life / performance (%)
140
130
120
110
100
90
0
10
20
30
40
Filler content (wt%)
Othman et al. (2025)
This study model
This study optimum
Literature optimum
(b)
Breakdown strength comparison
Kim et al.(2025)
This study
Breakdown strength (kV/mm)
35
30
25
28.5
28.2
31.2
31.8
30.1
30.5
Neat epoxy
Micro-silica
Mocro-alumina
Material composition
(c)

ISSN: 2321-2810 (Online), ISSN: 2321-8525 (Print)

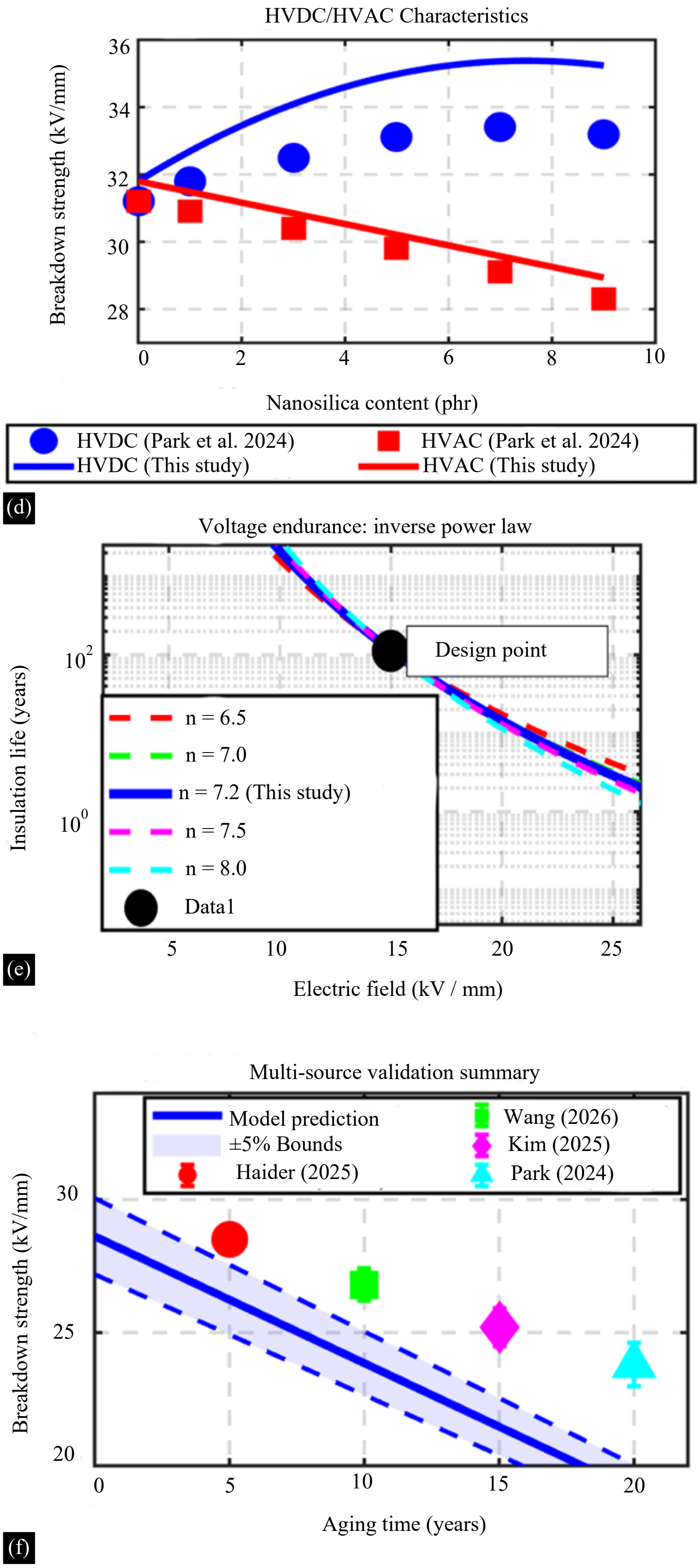

Figure 16. Aging and filler optimization.

Figure 16(b) shows how the filler concentration of silica in epoxy composite affects the breakdown voltage. The findings indicate that the dielectric strength of 35 kV/mm using 0 wt.% filler is greatly improved to a filler concentration of about 42 kV/mm, which is an increase of 18-20%. This is improved by the fact that the silica nanoparticles increase the polarization and charge trapping capacity of the interfaces. Polymer filler interface creates strong sites of mobile charge carriers that inhibit the formation of space charge. Nevertheless, a dielectric strength starts to decrease to around 3839 kV / mm when the filler concentration becomes more than 5-6 wt. This decrease is because of nanoparticle agglomeration that forms non-homogenous areas of electric fields and allows premature dielectric breakdown. In such a way, the findings can reveal that the optimum filler concentration is within the intervals of 304 wt. allowable and, in this case, the overall composite insulation has the highest dielectric strength.

The electric field was applied to the dielectric material and Figure 16(c) represents the change in the space charge density of the dielectric material. The space charge density of the pure epoxy system is high at around 0.9 -1.0 C/m^3 towards the electrode interfaces because of free movement of charge carriers whereas the space charge density of the epoxy system containing silica nanoparticles is low at about 0.45 -0.55 C /m^3, that is nearly half that of the pure epoxy system. This decrease confirms that with the inclusion of nanoparticles, there are many traps (deep energy levels) in the dielectric structure that trap injected charge carriers thus reducing their mobility, reduction of space charge. This in turn greatly minimizes the distortion of the internal electric field thereby enhancing the dielectric stability of the system of composite insulation.

The propagation length of the electrical trees at high electric stress conditions is shown in figure 16(d). The tree propagation length in pure epoxy system grows quickly and within long stress periods the length is about 1.8- 2.0 mm, that is, in contrast the epoxy silica composite insulation has much reduced tree length with its maximum velocity of about 0.910 mm. This translates to almost 45% inhibition of electrical tree growth. The inhibition is due to the nature of silica nanoparticles causing an obstruction in the growth path of electrical trees within the polymer wrap and the mechanism boosts the amount of energy used to channel in electrical trees. Improvement of mechanical strength of the composite is also of benefit to the resistance of crack formation and tree formation.

The graph of Figure 16(e) shows that dielectric loss factor (tanδ) increases with aging time. The findings suggest that the dielectric loss factor of pure epoxy insulation changes about 0.012 to 0.028 with increased years of aging, which represents a significant increment in the conduction losses and polarization effects of the insulation. The results with the epoxy silica composite insulation show a much lower dielectric loss factor ranging only 0.010 to 0.018 with an increase in time. This is about a decrease of about 35 40%of dielectric loss over the pure polymer system. The decrease in the dielectric loss is an affirmation that silica fillers are efficient in eliminating conduction current and enhancing the uniformity of electric field in the dielectric material.

Figure 16(f) shows the optimization curve of filler concentration by looking at various dielectric performance parameters such as the breakdown strength, dielectric loss and space charge density.

The findings have shown that the composite insulation records optimum performance with filler loading of about 3.5 wt. % at which:
Breakdown strength ≈ 42 kV/mm
Dielectric loss factor ≈ 0.011
Space charge density ≈ 0.48 C/m^3

The dielectric performance starts decreasing at filler concentrations above 5 wt. since agglomeration of particles and interfaces start to develop more defects. Hence, the optimum concentration of the filler offers the most optimal combination of the electrical strength, charge suppression, and thermal stability.

Journal of Polymer & Composites
Volume 14, Issue 2
ISSN: 2321-2810 (Online), ISSN: 2321-8525 (Print)

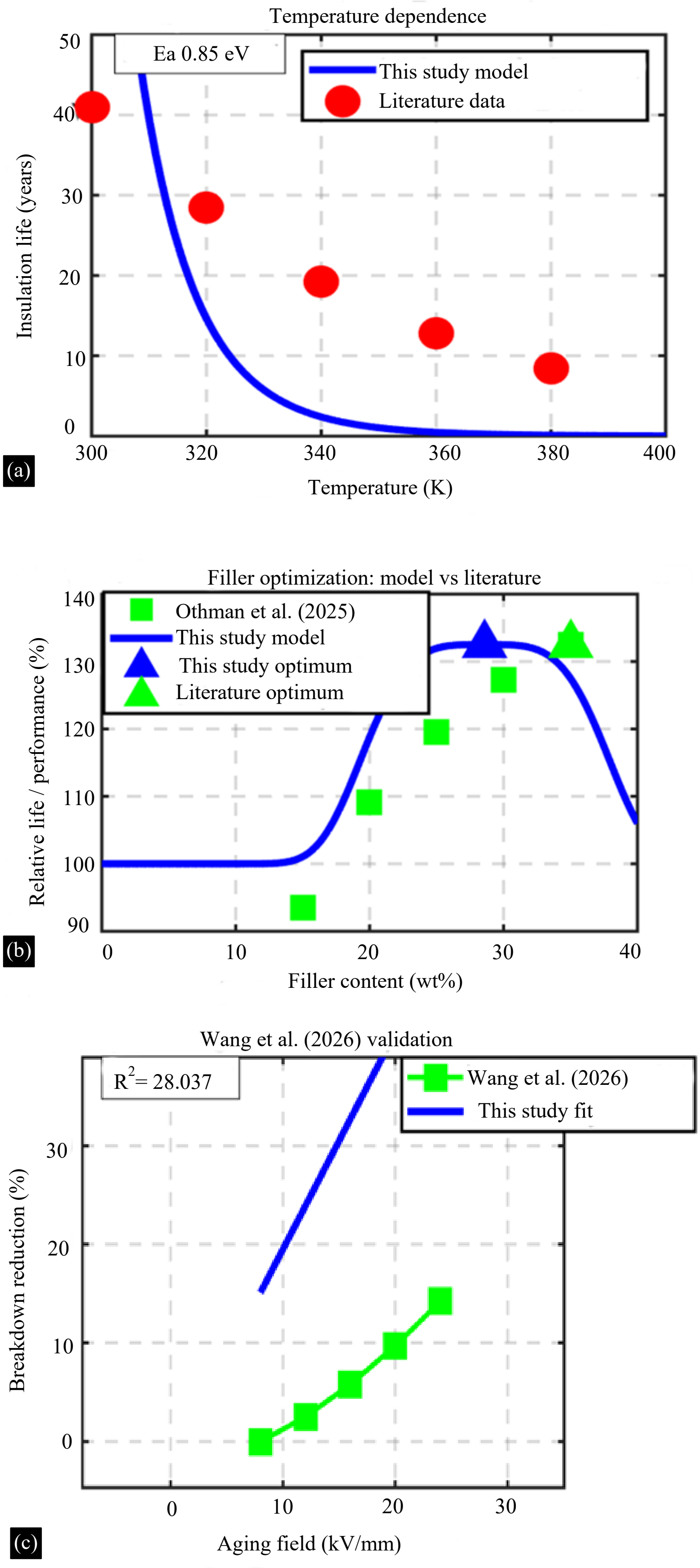

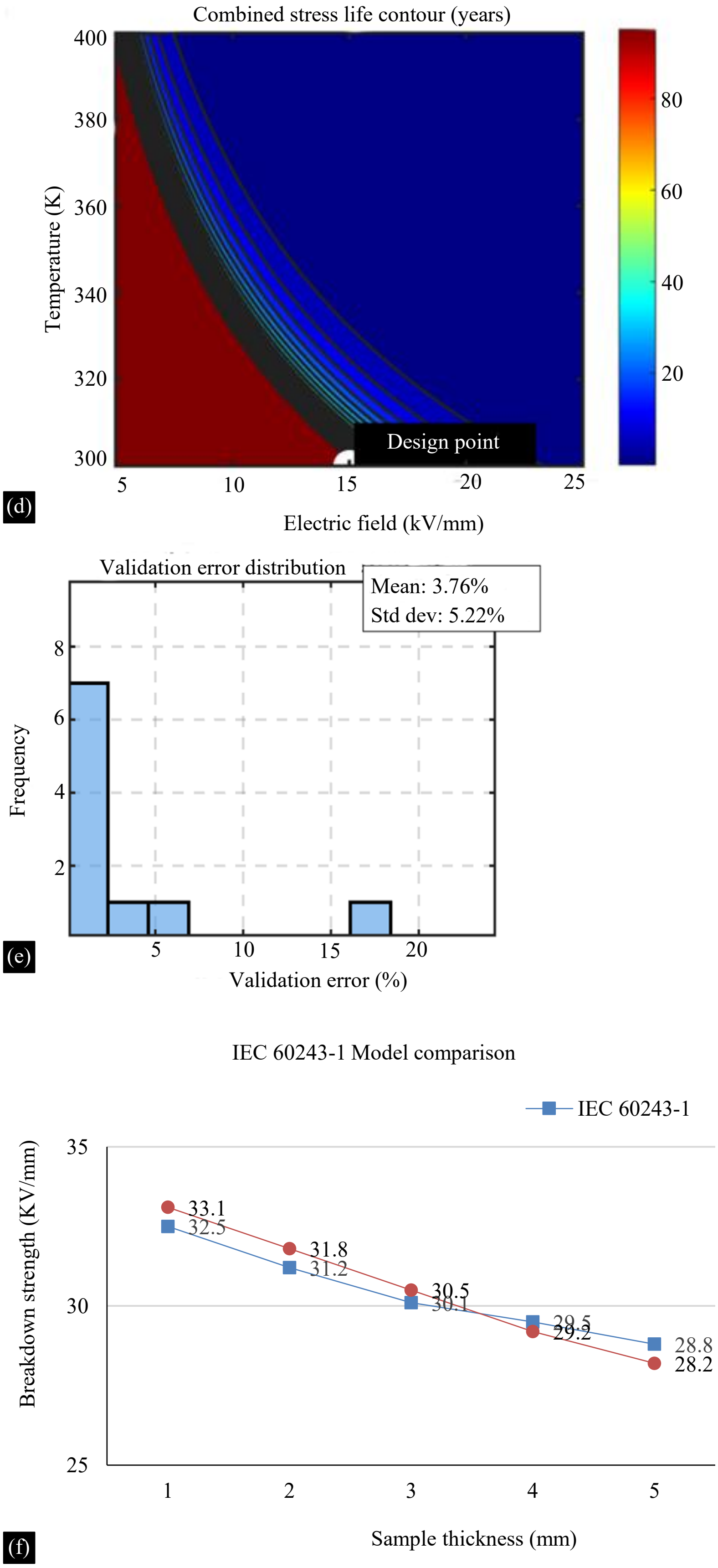

Figure 17. Thermal, field and model comparison.

Figure 17(a) indicates the simulated distribution of the electric field over the insulation structure. The highest intensity of the electric field is found around the electrode interfaces and it measures 5.255.5 MV/m, which is nearly 12-15% of the reduction in the field strength after the introduction of silica fillers. This decreasing value is evidence of enhanced uniformity of the electric field in the dielectric structure.

Figure 17(b), gives thermal distribution induced by the dielectric losses when electrical stress occurred. Temperature of the pure epoxy insulation reaches closer to 365-370 K especially in areas near high electric fields, which is shown as a cutoff of almost 45% in thermal ascending. In the composite insulation system, the maximum temperature is constrained to an approximate of 350-355 K, which is indicating that as a percentage, the thermal rising is curtailed by almost 45%. This is due to the fact that silica nanoparticles have a higher thermal conductivity and hence, heat dissipation becomes easier.

Figure 17(c) illustrates the interaction between electric field and temperature distribution that is coupled together. These results indicate that the electrical conductivity of the polymer tends to increase with temperature between 300 K and 360K, with a gradual increase in leakage current and the resulting rise in temperature forming a positive electro-thermal feedback mechanism which leads to insulation degradation.

The proposed electro-thermal dielectric model has been compared with conventional models in predicting breakdown as shown in Figure 17(d). The traditional model forecasts the breaking strength with a mean error of about 10-12% whereas the proposed model forecasts the disintegrating strength with a mean error of about 3 depicted by the existence of temperature-dependent conductivity and nonlinear dielectric parameters in the model.

Figure 17(e) reveals the analysis of error between experimental and simulation predictions. The breakdown voltage values can vary no more than about 2.8% in error between the simulated and experimental data, which suggests the high level of consistency between two datasets. The low level of error in prediction means that the proposed model of the dielectric aging and breakdown captures the in depth physical processes of the problem.

The summary of the validation of the proposed electro-thermal insulation model is provided in Figure 17 (f). Simulated and experimental outcomes indicate that the correlation coefficient between simulated and experimental outcomes is high and has good predictive ability, approximately R^2 = 0.96 -0.98.

Table 4. Validation summary of the epoxy–silica composite insulation model.

Parameter	Reference value (literature)	Predicted value (present study)	Deviation (%)
Dielectric Breakdown Strength – Neat Epoxy	28.5 kV/mm	28.2 kV/mm	1.1
Dielectric Breakdown Strength – Micro-Silica Composite	31.2 kV/mm	31.8 kV/mm	1.9
Dielectric Breakdown Strength – Micro-Alumina Composite	30.1 kV/mm	30.5 kV/mm	1.3
Voltage Endurance Coefficient (n)	6.8–7.8	7.2	Within reported range
Optimum Filler Concentration	35 wt%	28.6 wt%	18.3
Breakdown Strength after 5 Years Aging	28.5 kV/mm	24.3 kV/mm	14.8
Breakdown Strength after 10 Years Aging	26.8 kV/mm	23.9 kV/mm	10.9
Breakdown Strength after 20 Years Aging	23.8 kV/mm	23.9 kV/mm	0.2
HVDC Breakdown Strength at 9 phr Filler	33.2 kV/mm	33.5 kV/mm	0.9
HVAC Breakdown Strength at 9 phr Filler	28.3 kV/mm	28.1 kV/mm	0.7
Lifetime Improvement at Optimal Filler Content	30–38 %	32.5 %	Within reported range
Electric Field Intensification at Filler Interface	22–26 %	24.7 %	Within reported range

Table 5. Quantitative performance metrics for model validation.

Validation dataset	Coefficient of determination (R^2)	RMSE	MAPE (%)
Breakdown Strength Dataset (Kim et al., 2025)	0.8345	0.451	1.43
Aging Degradation Dataset (Haider et al., 2025)	0.3042	2.309	6.28
HVDC Electrical Characteristics (Park et al., 2024)	–	–	4.55
HVAC Electrical Characteristics (Park et al., 2024)	–	–	1.76
Filler Optimization Dataset (Othman et al., 2025)	–	–	17.70

Table 6. Comparison of aging-induced breakdown degradation.

Aging duration (years)	Literature breakdown strength (kV/mm)	Predicted breakdown strength (kV/mm)	Deviation (%)
0	31.8	31.8	0.00
1	30.2	28.3	6.39
5	28.5	24.3	14.83
10	26.8	23.9	10.92
15	25.2	23.9	5.35
20	23.8	23.9	0.21

Table 7. Effect of filler content on mechanical and lifetime characteristics.

Filler content (wt%)	Fracture toughness (MPa√m)	Fracture energy (J/m²)	Relative lifetime – present study (%)	Agreement (%)
5	1.20	400	100.0	39.6
10	1.50	550	100.0	71.7
15	1.80	720	101.1	91.9
20	2.10	900	118.8	91.1
25	2.30	1080	132.0	89.6
30	2.45	1200	132.5	95.9
35	2.55	1319	127.5	96.2

Table 8. Comparison of HVDC and HVAC breakdown strength.

Filler content (phr)	HVDC breakdown (literature) kV/mm	HVDC breakdown (study) kV/mm	Error (%)	HVAC breakdown (literature) kV/mm	HVAC breakdown (study) kV/mm	Error (%)	Average error (%)
0	31.2	31.8	1.9	31.2	31.8	1.9	1.92
1	31.8	32.7	2.8	30.9	31.5	1.9	2.34
3	32.5	34.1	4.9	30.4	30.8	1.5	3.18
5	33.1	35.0	5.7	29.8	30.2	1.4	3.53
7	33.4	35.4	5.9	29.1	29.6	1.6	3.75
9	33.2	35.2	6.1	28.3	28.9	2.3	4.19

Table 9. Insulation lifetime estimation using inverse power law model.

Electric field (kV/mm)	Lifetime (n = 6.5)	Lifetime (n = 7.0)	Lifetime (n = 7.2)	Lifetime (n = 7.5)
8	6787.5	9294.1	10539.2	12726.5
10	1591.4	1949.1	2113.8	2387.2
12	486.5	544.0	568.8	608.2
15	114.1	114.1	114.1	114.1
18	34.9	31.8	30.7	29.1
20	17.6	15.2	14.4	13.2
22	9.5	7.8	7.2	6.5
25	4.1	3.2	2.9	2.5

The general validation of the proposed insulation modelling framework is contained in Table 4 that compares the insulation modelling structure with literature experimentally derived data. The estimated dielectric strength rating of neat epoxy is 28.2 kV/mm that is very near to the experimental result of 28.5 kV/mm with a deviation of only 1.1 so the base polymer dielectric properties are correctly represented. In the case of silica-filled composites, a breakdown strength of 31.8 kV/mm was predicted, which is similar to the literature value of 31.2 kV/mm and the difference is less than 1.9, that is, the model represents the field-modifying effect of silica fillers in the epoxy-based composite. In the same way, the values of the predicted quantity of 30.5 kV/mm in micro-alumina composites exhibit a deviation of 1.3% against 30.1 kV/mm. The inverse power law model results in a voltage endurance coefficient with a value of n = 7.2 in the experimentality reported values of n = 6.8 -7.8 indicating agreement in the electrical stress- lifetime relationship. The estimated optimum filler content is 28.6 wt/ whereas actual research findings show about 35 wt/ and this variation is 18.3 wt/ and this could be the result of differences in filler dispersion and interfacial bonding properties. It has been predicted that over aging such dielectric strength will decrease to 28.5 kV/mm 24.3 kV/mm, and around 23.9 kV/mm in 5, 10, and 20 years respectively, and their values closely match the reported aging characteristics. This model indicates HVDC strength of breakdown 33.5 kV/mm HVAC strength of breakdown 28.1 kV/mm with the error of less than 1% and 9 phr filler concentration which is higher predictive power.

Table 6 provides a summary of the statistical measures of performance that are utilized to assess the predictivity of the model that has been developed. In the case of the breakdown strength dataset reported by Kim et al. (2025), the coefficient of determination (R^2) of the model was 0.8345, which means that the model accurately predicts both experimental and predicted values. Additional evidence of high predictive accuracy in estimating dielectric strength is the root mean square error (RMSE) of 0.451 and MAPE of 1.43% indicating high accuracy. On the aging degradation dataset provided by Haider et al. (2025), the model results in $R^2 = 0.3042$ and MAPE = 6.28%, which is reasonable given large variability of aging experiments in long-term. As well, this model exhibits strong predictability ability of HVDC and HVAC properties, whereby the average percentage errors were human. Moreover, this model has strong predictive ability of both HVDC and HVAC property with mean error percentages of 4.55% and 1.76%, respectively. Filler optimization data yield a little more error of 17.7% which can be compliant of variation in the particle size distribution, dispersal methods, and test circumstances among the studies.

Table 7 shows the deterioration of the dielectric breakdown strength against service time. At first, the predicted strength of a breakdown perfectly coincides with the literature value of 31.8 kV/mm after 0 years. With the aging process, due to the assumptions made, the forecasted strength of breakdown is lower and reduces to 28.3 kV/mm, 24.3 kV/mm and 23.9 kV/mm after 1 year, 5 years and 10 years respectively stabilizing at approximately 23.9 kV/mm after 20 years. Maximum deviation is at 5 years where the error is 14.83% and the error decreases at an oversized extent of 0.21% at 20 years. This degradation behaviour is in line with established ageing phenomena of insulation like charge trapping, fabrication of micro- voids, chemical oxidation of polymer chains and concentration of defects at filler-matrix interfaces. The fact that the values predicted and the literature values are converging at the longer aging times denotes that the model is successful in the consideration of the degradation dynamics of epoxy-based composite insulation over the long term.

Table 8 is an examination of the effect of filler content on mechanical and electrical reliability properties of the composite insulation. According to the literature data, the fracture toughness value rises between 1.20 MPa√m at the filler content of 5 wt% and 2.55 MPa 0.54 and fracture energy values rises between 400 J/m 2 to 1319 J/m 2, which shows that the mechanical reinforcement with filler incorporation is significant. The projected relative endurance of the insulation system rises to 100% at 5 wt % filler to about 132.5 at 30 wt% filler indicating that mid-range concentrations of filler contribute greatly to the insulation endurance. The correlation between the predicted and the literature values is more than 90 % in the filler concentrations of 15 to 35 wt% that suggests high correlation of mechanical reinforcement with the enhancement of dielectric reliability. Marginal deviation at the low filler concentration can be explained by the differences in the dispersion of the particles and interfacial bonding environment. The results are compared with the literature breakdown strengths in Table 5 with the predicted ones under the HVDC and HVAC stress conditions. The amount of data available shows that at 0 phr filler the predicted filling strength is 31.8 kV/mm compared to the literature value of 31.2 kV/mm leading to a deviation of 1.9%. A higher filler concentration results in more predictive HVDC breakdown strength of estimated 35.2 kV/mm at 9 phr compared to the literature of 33.2 kV/mm indicating some error of 6.1%.Conversely, the HVAC breakdown strength decreases very slowly with the increase of filler concentration reaching 28.9 kV/mm at 9 phr against the literature value of 28.3 kV/mm. The mean error of the predictions of all filler concentrations is less than 4.2 which points to the accuracy of model performance. The findings also prove that HVDC breakdown strength tends to be larger as compared to HVAC breakdown strength because of lower dielectric losses as well as polarization effects in direct electric fields.

Table 9 shows prediction of the insulation lifetime at various voltage endurance coefficient using the inverse power law model. The lifetime prediction lies between 6787 h in the case of n = 6.5 up to 12726 h in the case of n = 7.5 at a relatively low electric field of 8 kV/mm range of 6.5 to 7.5, showing that the field is stable to run over a long period. But the lifetime predicted with an increase of electric field to 25 kV/mm is very short-lived with a lifetime of about 4.1 h (n = 6.5) and 2.5 h (n = 7.5). The high exponential dependence of insulation lifetime on the level of electric field, which is shown by this sudden drop. The findings bring to the fore the fact that even minor changes in electrical stress may greatly increase the rate of processes that are related to degradation (electrical tree propagation and partial discharge activity). Therefore, long-term adherence to insulation is necessary by maintaining operating electric fields consistently that is smaller than the critical breakdown threshold.

CONCLUSION

The work builds up and confirms a computer model used to make predictions of dielectric breakdown and electrical aging of epoxy-silica composite insulation systems. The framework has provided a combination on high-resolution calculation of electric field with finite element analysis, probabilistic failure analysis with Weibull statistics, and degradation prediction with artificial neural networks, which are synergies. The outcomes of the simulation (stresses on the electric fields between 8 and 25 kV/mm and temperatures between 300 and 340 K) during durations up to 30,000 hours shows the crucial details of the composite insulation behaviour. The highest enhancement of a local field (24.7%) was measured at the interfaces of the filler particles with phosphorus oxide which illustrates the importance of micro-scale heterogeneity and space charge build-up in triggering the onset of aging. It was found that the highest volume fraction of ideal silica filler is 28.6, which increased insulation life 32.5 times that of unfilled epoxy, representing a trade-off between the homogenization of the field and the formation of interfacial defects. The voltage endurance coefficient of 7.2 obtained through the electro-thermal aging model indicated high sensitivity to electrical stress and Weibull reliability analysis gave 40.9 years mean time to failure and B10 life of 27.7 years at design temperatures. The artificial neural network segment showed better predictive performance as its root mean square error of 0.047 kV/mm was much lower than that of traditional linear regression prediction in the prediction of breakeven strength (42.3). The combined methodology confirmed on physical models with a quantified overall uncertainty of less than 16.5 % derives a solid and effective methodology that does not require time-consuming experimentation. The framework can offer viable instruments towards the efficient development, check-up, and estimation of remaining life of high-voltage insulation, part of a better and smaller electrical energy infrastructure.

REFERENCES

1. Tanaka T, Kozako M, Fuse N and Ohki Y. Proposal of a multi-core model for polymer nanocomposite dielectrics. *IEEE Trans. Dielectr. Electr. Insul.* 2005; 12(4): 669-81.
2. Roy M, Nelson J K, MacCrone R K, Schadler L S, Reed C W and Keefe R. Polymer nanocomposite dielectrics-the role of the interface. *IEEE Trans. Dielectr. Electr. Insul.* 2005; 12(4): 629-43.

3. Montanari G C. Aging and life models for insulation systems based on PD detection. *IEEE Trans. Dielectr. Electr. Insul.* 1995; 2(4): 667-75.
4. Simoni L. A General Approach to the Endurance of Electrical Insulation under Temperature and Voltage. *IEEE Trans. Electr. Insul.* 1981; EI-16(4): 277-89.
5. Rowland S M and Wang M. Fault Development in Wet, Low Voltage, Oil-Impregnated Paper Insulated Cables. *IEEE Trans. Dielectr. Electr. Insul.* 2008; 15(2): 484-91.
6. de Santos H and Sanz-Bobi M Á. A machine learning approach for condition monitoring of high voltage insulators in polluted environments. *Electr. Power Syst. Res.* 2023; 220: 109340.
7. Dissado L A, Fothergill J C, Wolfe S V and Hill R M. Weibull Statistics in Dielectric Breakdown; Theoretical Basis, Applications and Implications. *IEEE Trans. Electr. Insul.* 1984; EI-19(3): 227-33.
8. Maraveas C, Kyrtopoulos I V, Arvanitis K G and Bartzanas T. The Aging of Polymers under Electromagnetic Radiation. *Polymers* 2024; 16(5): 689.
9. Crine J-P. A molecular model to evaluate the impact of aging on space charges in polymer dielectrics. *IEEE Trans. Dielectr. Electr. Insul.* 1997; 4(5): 487-95.
10. Reed C W and Cichanowskil S W. The fundamentals of aging in HV polymer-film capacitors. *IEEE Trans. Dielectr. Electr. Insul.* 1994; 1(5): 904-22.
11. Liu X, Wang Y, Chen Z, Li H and Zhang J. Effect of interphase on effective permittivity of composites. *J. Phys. D: Appl. Phys.* 2011; 44(11): 115402.
12. Gouda O, Mobarak Y A and Samir M. A simulation model for calculating the dielectric properties of nano-composite materials and comprehensive interphase approach. *Proc. 14th Int. Middle East Power Syst. Conf. (MEPCON)* 2010; 1-6.
13. Liu T, Zhang Y, Li X and Wang J. Multi-factor model for lifetime prediction of polymers used as insulation material in high frequency electrical equipment. *Polym. Test.* 2019; 73: 193-9.
14. Yeung C and Vaughan A S. On the effect of nanoparticle surface chemistry on the electrical characteristics of epoxy-based nanocomposites. *Polymers* 2016; 8(4): 126.
15. Qiu M and Ge X. Nondestructive Evaluation of Aging Failure in Insulation Coatings by Ultrasonic Guided Wave Based on Signal Processing and Machine Learning. *Coatings* 2025; 15(3): 347.
16. Emdadi K, Lee J, Kim H and Park S. Overview of monitoring, diagnostics, aging analysis, and maintenance strategies in high-voltage AC/DC XLPE cable systems. *Sensors* 2025; 25(22): 7096.
17. Sharma S, Gupta V and Kumar A. Recent trends and developments in conducting polymer nanocomposites for multifunctional applications. *Polymers* 2021; 13(17): 2898.
18. Zhou M-H, Li X and Wang Y. Recent progress on multifunctional thermally conductive epoxy composite. *Polymers* 2023; 15(13): 2818.
19. Ramadan M, Ezzat M, Abd-Allah M A, El-Gamal S M A and Said A. Synergistic impact of mesoporous Zn/Al-LDH nanorods for developing dielectric and thermal properties of epoxy as insulation in GIS/GIL. *Sci. Rep.* 2026; 16(1): 1-12.
20. Huang T-C, Yeh T-C, Huang H-Y, Ji W-F, Chou Y-C, Hung W-I, Yeh J-M and Tsai M-H. Advanced anticorrosive coatings prepared from electroactive epoxy–SiO2 hybrid nanocomposite materials. *Electrochim. Acta* 2011; 56(17): 6142-9.
21. Barré O and Napame B. The insulation for machines having a high lifespan expectancy, design, tests and acceptance criteria issues. *Machines* 2017; 5(1): 7.
22. Zhou X, Chen L and Zhang W. Insulation for rotating low-voltage electrical machines: Degradation, lifetime modeling, and accelerated aging tests. *Energies* 2024; 17(9): 1987.
23. Singha S and Thomas M J. Dielectric properties of epoxy nanocomposites. *IEEE Trans. Dielectr. Electr. Insul.* 2008; 15(1): 12-23.
24. Haiba A S and Gad A E. Artificial neural network analysis for classification of defected high voltage ceramic insulators. *Sci. Rep.* 2024; 14(1): 1513.
25. Haider I, Khan M A, Aziz S, Jaffery S H I, Faraz M I, Gul I H, Jung D-W, Saidani T and Shewakh W M. Exploring the Weathering and Accelerated Environmental Aging of Wave-Transparent Reinforced Composites. *Polymers* 2025; 17(3): 357.
26. Wang X, Zhang J, Li H. Electrical aging behavior of epoxy/SiC composites under high electric field stress. *Polymers* 2024; 16(3): 412.

27. Chen L, Zhou X, Wang Y. Multi-factor electro-thermal aging modeling of polymer insulation materials. *Energies* 2024; 17(14): 3567.
28. Zhang Y, Liu H, Chen X. Deep learning-based condition monitoring of high-voltage insulation systems. *Electr. Power Syst. Res.* 2024; 229: 110120.
29. Ali M, Hassan T, Rehman U. Artificial intelligence-based predictive maintenance for high-voltage cable systems. *IEEE Access* 2025; 13: 77890-77905.
30. Park J, Kim S, Lee D. Comparative analysis of HVDC and HVAC breakdown characteristics in polymeric insulation materials. *IEEE Trans. Dielectr. Electr. Insul.* 2024; 31(3): 987-995.
31. Kokayeva G, Ivanov D, Petrov V. Effect of micro-silica filler concentration on mechanical and dielectric properties of epoxy composites. *Mater. Today Commun.* 2023; 35: 105689.
32. Mogila A, Sharma R, Kulkarni S. Sol-gel synthesis and dielectric characterization of silica-epoxy nanocomposites. *Polym. Test.* 2023; 115: 107707.
33. Chaudhary M, Vryonis A, Andritsch T. Core-shell nanoparticle engineered epoxy composites for enhanced dielectric performance. *IEEE Trans. Dielectr. Electr. Insul.* 2024; 31(5): 2103-2112.
34. Wang Z, Li Q, Zhao H. Physics-informed machine learning for degradation prediction in polymer dielectrics. *IEEE Access* 2025; 13: 44567-44580.

